Since January 2020 Elsevier has created a COVID-19 resource centre with free information in English and Mandarin on the novel coronavirus COVID-19. The COVID-19 resource centre is hosted on Elsevier Connect, the company's public news and information website.

CHAPTER 11

Detection of Analytes on Arrays/ Microarrays/DNA Chips

Chapter Outline

11.1 Introduction

In this chapter we use fractal analysis to analyze (a) the binding and dissociation (hybridization) of different targets (400 nM) in solution to a probe immobilized on a DNA chip surface (Fiche et al., 2007), (b) binding (hybridization) of different concentrations (in nM) of free-DNA in solution to a 22-mer strand (bound DNA) immobilized via a phenylene-diisocyanate linker molecule on a glass substrate (Michel et al., 2007), (c) binding (hybridization) of SA-HRP (streptavidin-horseradish peroxide) in solution to a capture probe on a QCM (quartz crystal microbalance) electrode along with a detection probe (Feng et al., 2007), (d) binding (hybridization) of a complementary and a noncomplementary (three-base mismatch strand) DNA in solution to a 30-mer 3′-thiolated DNA strand immobilized on an electrochemical enzymatic genosensor (Abad-Valle et al., 2007a,b), (e) binding (hybridization) of (i) a perfectly matched oligonucleotide (ODN-P) and (ii) a noncomplementary ODN (ODN-N) to an electrochemical sensor with a EST2-A34 reporter (Wang et al., 2007), (f) binding and dissociation during PNA-DNA hybridization—binding of different concentrations (in μM) of target DNA complementary to CYP2C9*2 (target DNA2) to CYP2C9*2 as a probe PNA immobilized on a ion-sensitive field-effect transistor (IS-FET)-based biosensor (Uno et al., 2007), (g) binding and dissociation during PNA-DNA hybridization—binding of different concentrations (in μM) of target DNA complementary to CYP2C9*2 (target DNA2) to CYP2C9*2 as a probe PNA

Handbook of Biosensors and Biosensor Kinetics. DOI: 10.1016/B978-0-444-53262-6.00011-5

immobilized on an IS-FET-based biosensor (Uno et al., 2007), (h) binding and dissociation of RNA synthesized on a (i) 42 nM template and a (ii) 420 nM template (Blair et al., 2007), and (i) binding (hybridization) of different concentrations of ss DNA in solution preincubated with prehybridized 22-nt FQ duplex to a "broken beacon" immobilized on a sensor surface (Blair et al., 2007). One may consider the fractal analysis as an alternate method of analyzing the kinetics of binding and dissociation during hybridization in these types of analyte-receptor reactions occurring on biosensor surfaces.

11.2 Theory

11.2.1 Single-Fractal Analysis

Binding Rate Coefficient

Havlin (1989) points out that the diffusion of a particle (analyte [Ag]) from a homogeneous solution to a solid surface (e.g., receptor [Ab]-coated surface) on which it reacts to form a product (analyte-receptor complex; Ab·Ag) is given by:

$$(\mathrm{Ab}\cdot\mathrm{Ag}) \approx \begin{cases} t^{(3-D_{\mathrm{f.bind}})/2} = t^{p}, & t < t_{\mathrm{c}} \\ t^{1/2}, & t > t_{\mathrm{c}} \end{cases} \tag{11.1}$$

Here $D_{\mathrm{f,bind}}$ or D_{f} is the fractal dimension of the surface during the binding step. t_{c} is the cross-over value. Havlin (1989) points out that the cross-over value may be determined by ${r_{\mathrm{c}}}^2 \sim t_{\mathrm{c}}$. Above the characteristic length, r_{c}, the self-similarity of the surface is lost and the surface may be considered homogeneous. Above time, t_{c} the surface may be considered homogeneous, since the self-similarity property disappears, and "regular" diffusion is now present. For a homogeneous surface where D_{f} is equal to 2, and when only diffusional limitations are present, $p = ½$ as it should be. Another way of looking at the $p = ½$ case (where $D_{\mathrm{f,bind}}$ is equal to two) is that the analyte in solution views the fractal object, in our case, the receptor-coated biosensor surface, from a "large distance." In essence, in the association process, the diffusion of the analyte from the solution to the receptor surface creates a depletion layer of width $(Đt)^{½}$ where Đ is the diffusion constant. This gives rise to the fractal power law, $(\mathrm{Analyte}\cdot\mathrm{Receptor}) \sim t^{(3-D_{\mathrm{f,bind}})/2}$. For the present analysis, t_{c} is arbitrarily chosen and we assume that the value of the t_{c} is not reached. One may consider the approach as an intermediate "heuristic" approach that may be used in the future to develop an autonomous (and not time-dependent) model for diffusion-controlled kinetics.

Dissociation Rate Coefficient

The diffusion of the dissociated particle (receptor [Ab] or analyte [Ag]) from the solid surface (e.g., analyte [Ag]-receptor [Ab]) complex coated surface) into solution may be given, as a first approximation by:

$$(\mathrm{Ab}\cdot\mathrm{Ag}) \approx -t^{(3-D_{\mathrm{f,diss}})/2} = -t^{p}, \quad t > t_{\mathrm{diss}} \tag{11.2}$$

Here $D_{f,diss}$ is the fractal dimension of the surface for the dissociation step. This corresponds to the highest concentration of the analyte-receptor complex on the surface. Henceforth, its concentration only decreases. The dissociation kinetics may be analyzed in a manner "similar" to the binding kinetics.

11.2.2 Dual-Fractal Analysis

Binding Rate Coefficient

Sometimes, the binding curve exhibits complexities and two parameters (k, D_f) are not sufficient to adequately describe the binding kinetics. This is further corroborated by low values of the r^2 factor (goodness-of-fit). In that case, one resorts to a dual-fractal analysis (four parameters; k_1, k_2, D_{f1}, and D_{f2}) to adequately describe the binding kinetics. The single-fractal analysis presented above is thus extended to include two fractal dimensions. At present, the time ($t = t_1$) at which the "first" fractal dimension "changes" to the "second" fractal dimension is arbitrary and empirical. For the most part, it is dictated by the data analyzed and experience gained by handling a single-fractal analysis. A smoother curve is obtained in the "transition" region,if care is taken to select the correct number of points for the two regions. In this case, the product (antibody-antigen; or analyte-receptor complex, Ab·Ag or analyte·receptor) is given by:

$$(\mathrm{Ab}\cdot\mathrm{Ag}) \approx \begin{cases} t^{(3-D_{f1,\mathrm{bind}})/2} = t^{p1}, & t < t_1 \\ t^{(3-D_{f2,\mathrm{bind}})/2} = t^{p2}, & t_1 < t < t_2 = t_c \\ t^{1/2}, & t > t_c \end{cases} \tag{11.3}$$

In some cases, as mentioned above, a triple-fractal analysis with six parameters (k_1, k_2, k_3, D_{f1}, D_{f2}, and D_{f3}) may be required to adequately model the binding kinetics. This is when the binding curve exhibits convolutions and complexities in its shape due perhaps to the very dilute nature of the analyte (in some of the cases to be presented) or for some other reasons. Also, in some cases, a dual-fractal analysis may be required to describe the dissociation kinetics.

11.3 Results

We will use fractal analysis to analyze the binding (hybridization) and dissociation kinetics exhibited by different analyte-receptor reactions occurring on biosensor surfaces. This is just one possible method of analyzing the kinetics of the different analyte-recptor (hybridization reactions) presented in this chapter. Alternative expressions for fitting the data are available that include saturation, first-order reaction, and no diffusion limitations, but these expressions are apparently deficient in describing the heterogeneity that inherently exists on the surface. One might justifiably argue that the appropriate modeling may be achieved by using a Langmuirian or other approach. The Langmuirian approach may be used to model the data presented if one assumes the presence of discrete classes of sites (for example, double

exponential analysis as compared with a single-fractal analysis). Lee and Lee (1995) report that the fractal approach has been applied to surface science, for example, adsorption and reaction processes. These authors point out that the fractal approach provides a convenient means to represent the different structures and the morphology at the reaction surface. They also draw attention to the use of the fractal approach to develop optimal structures and as a predictive approach. Another advantage of the fractal technique is that the analyte-receptor association (as well as the dissociation reaction) is a complex reaction, and the fractal analysis via the fractal dimension and the rate coefficient provides a useful lumped parameter(s) analysis of the diffusion-limited reaction occurring on a heterogeneous surface.

In a classical situation, to demonstrate fractality, one should make a log-log plot, and one should definitely have a large amount of data. It may be useful to compare the fit to some other forms, such as exponential, or one involving saturation, etc. At present, no independent proof or physical evidence of fractals in the examples is presented. It is a convenient means (since it is a lumped parameter) to make the degree of heterogeneity that exists on the surface more quantitative. Thus, there is some arbitrariness in the fractal model to be presented. The fractal approach provides additional information about interactions that may not be obtained by conventional analysis of biosensor data.

There is no nonselective adsorption of the analyte. The present system being analyzed may be typically very dilute. Nonselective adsorption would skew the results obtained very significantly. In these types of systems, it is imperative to minimize this nonselective adsorption. It is also recognized that, in some cases, this nonselective adsorption may not be a significant component of the adsorbed material and that this rate of association, which is of a temporal nature, would depend on surface availability. If the nonselective adsorption were to be accommodated into the model, there would be an increase in the heterogeneity on the surface, as, by its very nature, nonspecific adsorption is more homogeneous than specific adsorption. This would lead to higher fractal dimension values since the fractal dimension is a direct measure of the degree of heterogeneity that exists on the surface.

Fiche et al. (2007) recently analyzed hybridization experiments on a DNA chip using surface plasmon resonance imaging (SPRi). These authors point out that to obtain quantitative results it is essential to clarify the heterogeneity of the hybridization of DNA on microarrays. The aim of their experiment was to obtain a detailed account of the equilibrium and kinetics of hybridization on a DNA chip. They point out that experimental results on a DNA chip are commonly analyzed using the Langmuir model (Peterson et al., 2002; Hekstra et al., 2003; Tawa and Knoll, 2004; Yu et al., 2004; Wark et al., 2005; Yao et al., 2005). In most of the above mentioned studies the heterogeneity of the hybridization is generally not taken into account. Furthermore, Fiche et al. (2007) explain that as most of the experiments are done at room temperature effects on the equilibrium and kinetics properties are not taken into account. Thus, these authors analyzed temperature effects on DNA experiments.

Fiche et al. (2007) performed hybridization experiments at different temperatures and target concentrations. All their probes had at their 5′end a 10-thyminespacer and a pyrrole (Py) moiety for the electropolymerization grafting method. Figure 11.1a shows the binding and dissociation of the target T1 to the probe P14 (5′-Py-(T_{10})-GCC.TGG.ACG.ATA.CA-3′) immobilized on the DNA chip. 14 refers to the number of hybridizing bases. A dual-fractal analysis is required to adequately describe the binding kinetics. A single-fractal analysis is adequate to describe the dissociation kinetics. The values of (a) the binding rate coefficient, k, and the fractal dimension, D_f, for a single-fractal analysis, (b) the binding rate coefficients, k_1 and k_2, and the fractal dimensions, D_{f1} and D_{f2}, for a dual-fractal analysis, and the dissociation rate coefficient, k_d and the fractal dimension for dissociation, D_{fd} are given in Table 11.1. The values of the binding and the dissociation rate coefficients, and the fractal dimensions for the binding and the dissociation phase presented in Table 11.1 were obtained from a regression analysis

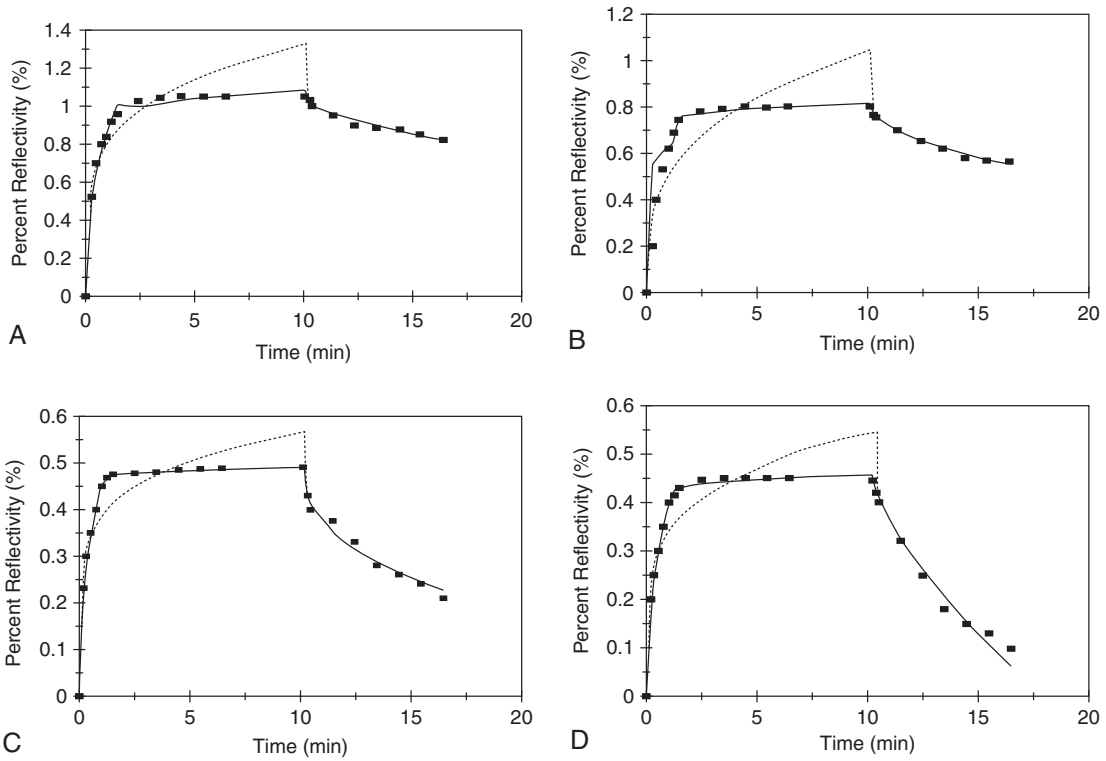

Figure 11.1

Binding and dissociation (hybridization) of different targets (400 nM) in solution to a probe immobilized on a DNA chip surface at 32.5 °C (Fiche et al., 2007): (a) P14. (b) P12. (c) P10. (d) P9. When only a solid line (—) is used then a single-fractal analysis applies. When both a dashed (- - -) and a solid (—) line are used then the dashed line represents a single-fractal analysis and the solid line represents a dual-fractal analysis.

Table 11.1: Binding and dissociation rate coefficients and fractal dimensions for the binding and the dissociation phase during hybridization on a DNA chip (Fiche et al., 2007).

Target/Probe	k	k_1	k_2	k_d	D_f	D_{f1}	D_{f2}	D_{fd}
400 nM T1/ P14	0.8028 ± 0.0774	0.8623 ± 0.0445	0.9422 ± 0.0268	2.807 ± 0.051	2.5632 ± 0.06376	2.2344 ± 0.1346	2.8783 ± 0.0292	3.0- 0.0774
400 nM T1/ P12	0.5051 ± 0.1408	0.6261 ± 0.0849	0.7441 ± 0.0119	0.0941 ± 0.0052	2.3744 ± 0.1346	2.3744 ± 0.1346	2.9218 ± 0.0204	1.9260 ± 0.0312
400 nM T1/ P10	0.1235 ± 0.0152	0.4545 ± 0.021	0.4693 ± 0.0016	0.1235 ± 0.0152	2.6704 ± 0.05926	2.6704 ± 0.0593	2.9594 ± 0.0037	2.1790 ± 0.06688
400 nM T1/P9	0.1057 ± 0.0104	0.3995 ± 0.0096	0.4230 ± 0.0076	0.1057 ± 0.0104	2.6186 ± 0.0606	2.6186 ± 0.0606	2.9301 ± 0.0185	1.5948 ± 0.05398

using Corel Quattro Pro 8.0 (1997) to model the experimental data using Equations (11.1)–(11.3), wherein [analyte·receptor or Ab·Ag] $= kt^p$ for the binding step, and [analyte·receptor or Ab·Ag]$= -kt^p$ for the dissociation step.

The binding and the dissociation rate coefficients presented in Table 11.1 are within 95% confidence limits. For example, for the binding of 400 nM target T1 in solution to the probe P14 immobilized on a DNA sensor chip the binding rate coefficient, k_1, value for a dual-fractal analysis is 0.8623 ± 0.0445. The 95% confidence limit indicates that the k_1 values will lie between 0.8178 and 0.90968. This indicates that the values are precise and significant. To indicate the goodness-of-fit, the r^2 value is provided. In this case the r^2 value is 0.961. This is a typical value obtained.

Figure 11.1b shows the binding and dissociation of the target T1 to the probe P12 (5′-Py-(T_{10})-GCC.TGG.ACG.ATA-3′) immobilized on the DNA chip. 12 refers to the number of hybridizing bases. Once again, a dual-fractal analysis is required to adequately describe the binding kinetics. A single-fractal analysis is adequate to describe the dissociation kinetics. The values of (a) the binding rate coefficient, k, and the fractal dimension, D_f, for a single-fractal analysis, (b) the binding rate coefficients, k_1 and k_2, and the fractal dimensions, D_{f1} and D_{f2}, for a dual-fractal analysis, and the dissociation rate coefficient, k_d and the fractal dimension for dissociation, D_{fd} are given in Table 11.1.

Figure 11.1c shows the binding and dissociation of the target T1 to the probe P10 (5′-Py-(T_{10})-GCC.TGG.ACG.A-3′) immobilized on the DNA chip. 10 refers to the number of hybridizing bases. Once again, a dual-fractal analysis is required to adequately describe the binding kinetics. A single-fractal analysis is adequate to describe the dissociation kinetics. The values of (a) the binding rate coefficient, k, and the fractal dimension, D_f, for a single-fractal analysis, (b) the binding rate coefficients, k_1 and k_2, and the fractal dimensions, D_{f1} and D_{f2}, for a dual-fractal analysis, and the dissociation rate coefficient, k_d and the fractal dimension for dissociation, D_{fd} are given in Table 11.1.

Figure 11.1d shows the binding and dissociation of the target T1 to the probe P9 (5′-Py-(T_{10})-GCC.TGG.ACG-3′) immobilized on the DNA chip. 9 refers to the number of hybridizing bases. Once again, a dual-fractal analysis is required to adequately describe the binding kinetics. A single-fractal analysis is adequate to describe the dissociation kinetics. The values of (a) the binding rate coefficient, k, and the fractal dimension, D_f, for a single-fractal analysis, (b) the binding rate coefficients, k_1 and k_2, and the fractal dimensions, D_{f1} and D_{f2}, for a dual-fractal analysis, and the dissociation rate coefficient, k_d and the fractal dimension for dissociation, D_{fd} are given in Table 11.1.

Figure 11.2a and Table 11.1 show for the binding of different targets (400 nM) in solution to a probe immobilized on a DNA chip surface at 32.5 °C and for a dual-fractal analysis the decrease in the binding rate coefficient, k_2, with an increase in the fractal

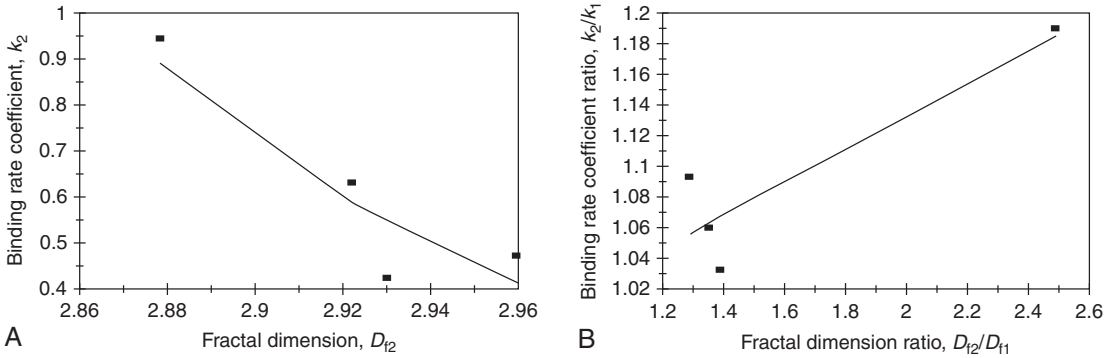

Figure 11.2

(a) Decrease in the binding rate coefficient, k_2, with an increase in the fractal dimension, D_{f2}. Increase in the ratio of the binding rate coefficients, k_2/k_1, with an increase in the ratio of fractal dimensions, D_{f2}/D_{f1}.

dimension, D_{f2}. For the data shown in Figure 11.2a, the binding rate coefficient, k_2, is given by:

$$k_2 = [3.6 \pm 0.8 \times 10^{12}] D_{f2}^{-27.46 \pm 10.45} \tag{11.4a}$$

The fit is good. Only four data points are available. The availability of more data points would lead to a more reliable fit. The binding rate coefficient, k_2, is extremely sensitive to the degree of heterogeneity on the biosensor surface or the fractal dimension, D_{f2}, as noted by the negative order close to twenty seven and a half (equal to -27.46) exhibited.

Figure 11.2b also shows the increase in the ratio of the binding rate coefficients, k_2/k_1, with an increase in the ratio of the fractal dimensions, D_{f2}/D_{f1}, for the binding of different targets (400 nM) in solution to a probe immobilized on a DNA chip surface at 32.5 °C and for a dual-fractal analysis. For the data shown in Figure 11.2b, the ratio of the binding rate coefficients, k_2/k_1, is given by:

$$k_2/k_1 = (1.0094 \pm 0.0362)(D_{f2}/D_{f1})^{0.174 \pm 0.0656} \tag{11.4b}$$

The fit is reasonable. Only four data points are available. The availability of more date points would lead to a more reliable fit. The ratio of the binding rate coefficients, k_2/k_1, exhibit only a mild order (equal to 0.174) of dependence on the ratio of the fractal dimensions, D_{f2}/D_{f1}.

Michel et al. (2007) recently reported that microarrays can readily identify DNA sequences simultaneously, and are rapidly becoming major tools for pharmacogenomics and clinical pathology. These authors used an optical method to analyze the DNA surface hybridization. They noted that DNA surface density is a key parameter in microarray hybridization kinetics.

Also, a change in the bulk concentration has a significant impact on hybridization kinetics. They analyzed hybridization kinetics on glass substrates. One 22-mer strand (bound DNA) was immobilized via a phenylene-diisocyanate linker molecule on the glass substrate. The dye-labeled (Cy3) complementary strand was in solution in a reaction chamber. These authors further explain that to work efficiently with microarrays a knowledge of kinetics and thermodynamics is essential.

Figure 11.3a shows the binding of 10 nM free-DNA in solution to a 22-mer strand (bound DNA) immobilized via a phenylene-diisocyanate linker molecule on a glass substrate (Michel et al., 2007). A dual-fractal analysis is required to adequately describe the binding kinetics. The values of (a) the binding rate coefficient, k, and the fractal dimension, D_f, for a single-fractal analysis and (b) the binding rate coefficients, k_1 and k_2, and the fractal dimensions, D_{f1} and D_{f2}, for a dual-fractal analysis are given in Table 11.2.

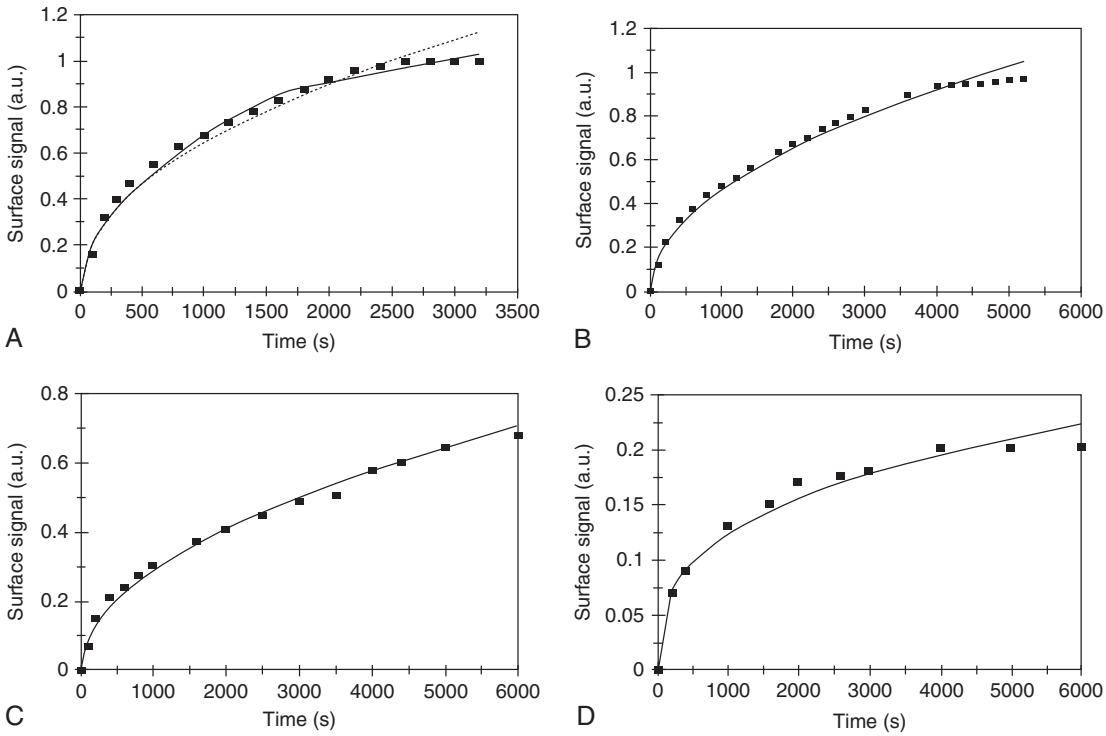

Figure 11.3

Binding (hybridization) of different concentrations (in nM) of free-DNA in solution to a 22-mer strand (bound DNA) immobilized via a phenylene-diisocyanate linker molecule on a glass substrate (Michel et al., 2007): (a) 10. (b) 7.5. (c) 5. (d) 2. When only a solid line (—) is used then a single-fractal analysis applies. When both a dashed (- - -) and a solid (—) line are used then the dashed line represents a single-fractal analysis and the solid line represents a dual-fractal analysis.

Table 11.2: Binding rate coefficients and fractal dimensions for different initial-free DNA concentrations (in nM) on a substrate prepared following protocol A (Michel et al., 2007).

Initial Free-DNA Concentration (nM)	k	k_1	k_2	D_f	D_{f1}	D_{f2}
10	0.02345 ± 0.0019	0.01789 ± 0.00190	0.1193 ± 0.0031	2.0390 ± 0.04794	1.9482 ± 0.0640	2.4652 ± 0.07622
7.5	0.01509 ± 0.001	na	na	2.0062 ± 0.02562	na	na
5	0.009188 ± 0.000959	na	na	2.0004 ± 0.04282	na	na
2	0.01326 ± 0.00083	na	na	2.3518 ± 0.03674	na	na

Note that an increase in the fractal dimension by a factor of 1.265 from a value of D_{f1} equal to 1.9482 to D_{f2} equal to 2.465 leads to an increase in the binding rate coefficient by a factor of 6.67 from a value of k_1 equal to 0.01789 to k_2 equal to 0.1193.

Figure 11.3b shows the binding of 7.5 nM free-DNA in solution to a 22-mer strand (bound DNA) immobilized via a phenylene-diisocyanate linker molecule on a glass substrate (Michel et al., 2007). A dual-fractal analysis is required to adequately describe the binding kinetics. The values of (a) the binding rate coefficient, k, and the fractal dimension, D_f, for a single-fractal analysis and (b) the binding rate coefficients, k_1 and k_2, and the fractal dimensions, D_{f1} and D_{f2}, for a dual-fractal analysis are given in Table 11.2.

Figure 11.3c shows the binding of 5.0 nM free-DNA in solution to a 22-mer strand (bound DNA) immobilized via a phenylene-diisocyanate linker molecule on a glass substrate (Michel et al., 2007). A dual-fractal analysis is required to adequately describe the binding kinetics. The values of (a) the binding rate coefficient, k, and the fractal dimension, D_f, for a single-fractal analysis and (b) the binding rate coefficients, k_1 and k_2, and the fractal dimensions, D_{f1} and D_{f2}, for a dual-fractal analysis are given in Table 11.2.

Figure 11.3d shows the binding of 2.0 nM free-DNA in solution to a 22-mer strand (bound DNA) immobilized via a phenylene-diisocyanate linker molecule on a glass substrate (Michel et al., 2007). A dual-fractal analysis is required to adequately describe the binding kinetics. The values of (a) the binding rate coefficient, k, and the fractal dimension, D_f, for a single-fractal analysis and (b) the binding rate coefficients, k_1 and k_2, and the fractal dimensions, D_{f1} and D_{f2}, for a dual-fractal analysis are given in Table 11.2.

Figure 11.4 and Table 11.2 show for a single-fractal analysis the decrease in the fractal dimension, D_f with an increase in the initial free-DNA concentration in the 2-7.5 nM range in solution. For this 2-7.5 nM concentration range, the fractal dimension, D_f, is given by:

$$D_f = (2.547 \pm 0.107)[\text{initial free} - \text{DNA, in nM}]^{-0.1298 \pm 0.0429} \qquad (11.4c)$$

The fit is good. Only three data points are available. The availability of more data points would lead to a more reliable fit. The fractal dimension, D_f, exhibits a very slight negative order (equal to -0.1298) of dependence on the initial free-DNA concentration in solution. The fractal dimension, D_f, is based on a log scale. Thus, even very small changes in the fractal dimension indicate significant changes in the degree of heterogeneity on the biosensor chip surface.

Figure 11.5 shows the binding of 1 nM initial free-DNA concentration in solution at 22 mer strand (bound DNA) immobilized via a phenylene-diisocyanate linker molecule on a glass substrate (Michel et al., 2007). A single-fractal analysis is adequate to describe the binding kinetics. The values of the binding rate coefficient, k, and the fractal dimension, D_f, are given in Table 11.3.

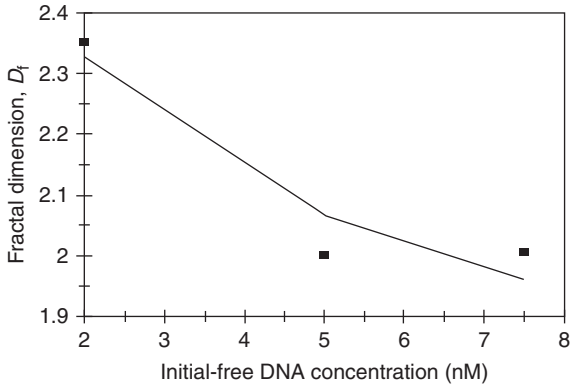

Figure 11.4
Decrease in the fractal dimension, D_f, with an increase in the free-DNA concentration (in nM) in solution.

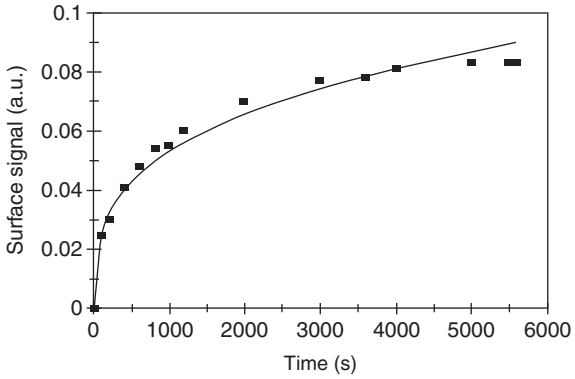

Figure 11.5
Binding (hybridization) of 1 nM free-DNA concentration in solution to a 22 mer strand (bound DNA) immobilized via a phenylene-diisocyanate linker molecule on a glass substrate (Michel et al., 2007).

Figure 11.6a shows the binding of nonmatching, noncomplementary strand m22 5′-Cy3-TGA GCG TTC GTG GTG GGA TAG T-3′ in solution to one strand (bound DNA; i22, 5′-NH_2-C6-TTT TTT TTT TTT TTT TGA TAG GGT GGT GCT GGT GCT TGC GAG T-3′) immobilized on a glass substrate (Michel et al., 2007). A single-fractal analysis is adequate to describe the binding kinetics. The values of the binding rate coefficient, k, and the fractal dimension, D_f, for a single-fractal analysis are given in Table 11.3.

Figure 11.6b shows the binding of a matching sequence, complementary strand p22 5′-Cy3-ACT CGC AAG CAC CAC CCT ATC-A-3′ in solution to one strand (bound DNA; i22, 5′-NH_2-C6 TTT TTT TTT TTT TTT TGA TAG GGT GGT GCT GGT GCT TGC GAG T-3′) immobilized

Table 11.3: Binding rate coefficients and fractal dimensions for (a) bulk concentration of free DNA in solution (1 nM) to sensor surface, (b) nonmatching (non complementary; m22; 5′-Cy3-TGA-GCG-TTC-GTG-GTG-GGA-TAG-T-3′), and matching sequence (complementary; p22; 5′-Cy3-ACT-CGC-AAG-CAC-CAC-CCT-ATC-A-3′) in solution to one strand (bound DNA; i22; 5′-NH_2-C6-TTT-TTT-TTT-TTT-TTT-TGA-TAG-GGT-GGT-GCT-GGT-GCT-TGC-GAG-T-3′) immobilized on a glass substrate (Michel et al., 2007).

Strand in Solution/ Receptor on Surface	k	k_1	k_2	D_f	D_{f1}	D_{f2}
1 nM free DNA/ surface	0.006628 ± 0.000415	na	na	2.3966 ± 0.02612	na	na
Noncomplementary (m22)/i22	$5.7 \times 10^{-05} \pm 3 \times 10^{-05}$	na	na	1.7036 ± 0.1151	na	na
Complementary (p22)/i22	0.06240 ± 0.01266	0.008629 ± 0.000020	0.4462 ± 0.0162	2.2074 ± 0.1243	1.4592 ± 0.005772	2.7794 ± 0.05058

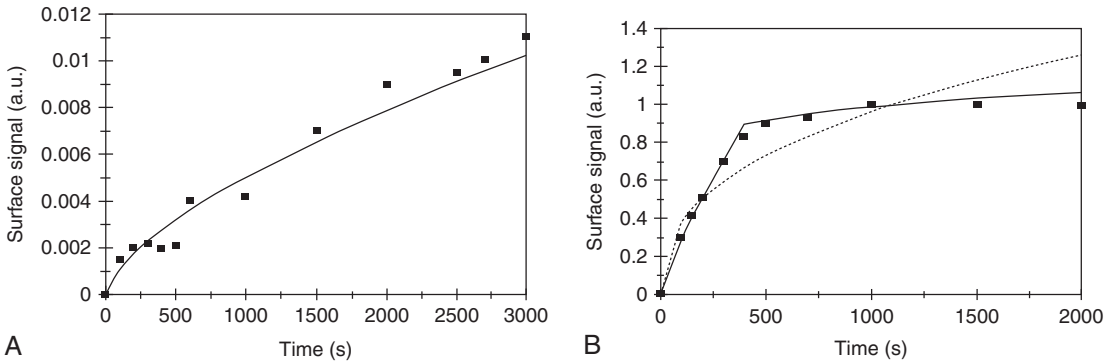

Figure 11.6

Binding of 100 nM free-DNA in solution to a (a) noncomplementary and (b) a complementary 22 mer strand (bound DNA) immobilized via a phenylene-diisocyanate linker molecule on a glass substrate (Michel et al.,2007). When only a solid line (—) is used then a single-fractal analysis applies. When both a dashed (- - -) and a solid (—) line are used then the dashed line represents a single-fractal analysis and the solid line represents a dual-fractal analysis.

on a glass substrate (Michel et al., 2007). A dual-fractal analysis is required to adequately describe the binding kinetics. The values of (a) the binding rate coefficient, k, and the fractal dimension, D_f, for a single-fractal analysis, and the binding rate coefficients, k_1 and k_2, and the fractal dimensions, D_{f1} and D_{f2}, for a dual-fractal analysis are given in Table 11.3. It is of interest to note that for a dual-fractal analysis, as the fractal dimension increases by a factor of 1.905 from a value of D_{f1} equal to 1.4592 to D_{f2} equal to 2.7794, the binding rate coefficient increases by a factor of 51.71 from a value of k_1 equal to 0.00869 to k_2 equal to 0.4462.

Also note that for the binding in the nonmatching (noncomplementary) case a single-fractal analysis is adequate to describe the binding kinetics. However, for the matching (complementary) case a dual-fractal analysis is required to describe the binding kinetics. This would indicate that, at least for this case, the binding of the matching (complementary) case is more complicated than that of the nonmatching (noncomplementary) case. No explanation is offered, at present, to help explain why this is the case.

Feng et al. (2007) recently reported that single nucleotide polymorphisms (SNPs) are important in clinical diagnostics, pathology detection, and genetic diseases. Lin et al. (2005) point out that SNPs are point mutations that include the most-common genetic variation. Wabuyele et al. (2003) have explained that quite a few genetic diseases and cancers are associated with mutation in the sequence of particular genes. Landegren et al. (1988) initially used DNA ligase for the detection of SNPs. Feng et al. (2007) have used the QCM technique coupled with the DNA enzyme-based ligase reaction to sense a point mutation in a DNA target. These authors used a signal amplification method for the quantitative detection of the target gene that included the deposition of an insoluble product of 3,3-diaminobenzidine (DAB) (Karousis et al., 2002) on the electrode supports mediated by SA-HRP conjugate.

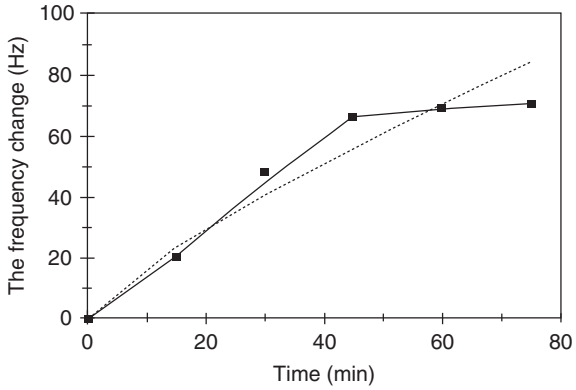

Figure 11.7

Binding (hybridization) of SA-HRP (streptavidin horseradish peroxidase) in solution to a capture probe on a QCM (quartz crystal microbalance) electrode along with a detection probe (Feng et al., 2007). When only a solid line (—) is used then a single-fractal analysis applies. When both a dashed (- - -) and a solid (—) line are used then the dashed line represents a single-fractal analysis and the solid line represents a dual-fractal analysis.

Figure 11.7a shows the binding of SA-HRP and DAB in solution to the capture probe modified QCM electrode along with 1 μM detection probe. A dual-fractal analysis is required to adequately describe the binding kinetics. The values of (a) the binding rate coefficient, k, and the fractal dimension, D_f, for a single-fractal analysis, and (b) the binding rate coefficients, k_1 and k_2 and the fractal dimensions, D_{f1} and D_{f2}, for a dual-fractal analysis are given in Tables 11.4 and 11.5. It is of interest to note that for a dual-fractal analysis as the fractal dimension increases by a factor of 3.51 from a value of D_{f1} equal to 0.7886 to D_{f2} equal to 2.7684, the binding rate coefficient increases by a factor of 41.96 from a value of k_1 equal to 1.0132 to k_2 equal to 42.513.

Abad-Valle et al. (2007a,b) recently used an electrochemical enzymatic genosensor to analyze DNA single-base mismatches. These authors report that electrochemical transducers provide rapid and sensitive measurements. Besides, these devices are simple low cost, and exhibit the potential to be miniaturized. Abad-Valle et al. (2005) further explain that enzyme labels, due to their inherent amplification help permit an increase in assay sensitivity. Caruana and Heller (1999) used a soybean peroxidase label for detecting a single-base mismatch in an 18-base oligonucleotide. Abad-Valle et al. (2005) had previously developed an enzymatic electrochemical genosensor on gold films to analyze the selectivity of DNA hybridization. Abad-Valle et al. (2007a,b) report that they have used a sequence of the SARS (severe acute respiratory syndrome) coronavirus (CoV) as a target. This SARS CoV is the causative agent of an atypical pneumonia. They further point out that it is essential to identify the SARS-CoV quickly and accurately owing to the rate of mortality of patients.

Table 11.4: Binding and dissociation rate coefficients for the hybridization of different analytes in solution to complementary or noncomplementary receptors immobilized on different biosensor surfaces.

Biosensor Type	Analyte in Solution/ Receptor on surface	k	k_1	k_2	k_3	k_d	References
QCM	3,3-diaminobenzidine/ sterptavidin-peroxide horseradish (SA-HRP)	2.7136 ± 0.5831	1.0132 ± 0.1069	42.513 ± 0.141	na	na	Feng et al. (2007)
Electrochemical enzymatic genosensor	Sequence of the SARS (severe acute respiratory syndrome) coronavirus (CoV) SARS-CoV/(c-DNA) 30-mer 3′-thiolated DNA strand	7.0291 ± 1.1079	na	na	na	na	Abad-Valle et al. (2007a,b)
Electrochemical enzymatic genosensor	Sequence of the SARS (severe acute respiratory syndrome) coronavirus (CoV) SARS-CoV/3 base mismatch 30-mer 3′-thiolated DNA strand	23.569 ± 2.627	na	na	na	na	Abad-Valle et al. (2007a,b)
Electrochemical detection	*p*-aminophenylbutyrate/ esterase 2 from *Alicyclobacillus acidocaldarius* plus oligodeoxynucleotide (ODN) in a site-specific manner (perfectly matched; ODN-P)	6.9462 ± 1.9652	2.8403 ± 0.2542	37.626 ± 1.136	na	0.07685 ± 0.00598	Wang et al. (2007)
Electrochemical detection	*p*-aminophenylbutyrate/ esterase 2 from *Alicyclobacillus acidocaldarius* plus oligodeoxynucleotide (ODN) in a site-specific manner (noncomplementary ODN; ODN-N)	0.1261 ± 0.0600	0.0409 ± 0.0135	1.5596 ± 0.1142	4.7240 ± 0.4477	na	Wang et al. (2007)

Table 11.5: Fractal dimensions for the binding and the dissociation phases for the hybridization of different analytes in solution to complementary or noncomplementary receptors immobilized on different biosensor surfaces.

Biosensor Type	Analyte in Solution/ Receptor on Surface	D_f	D_{f1}	D_{f2}	D_{f3}	D_{fd}	References
QCM	3,3-diaminobenzidine/ sterptavidin-peroxide horseradish (SA-HRP)	1.4132 ± 0.3062	0.7886 ± 0.2512	2.7684 ± 0.01818	na	na	Feng et al. (2007
Electrochemical enzymatic genosensor	Sequence of the SARS (severe acute respiratory syndrome) coronavirus (CoV) SARS-CoV/(c-DNA) 30-mer 3′-thiolated DNA strand	1.9290 ± 0.2812	na	na	na	na	Abad-Valle et al. (2007a,b)
Electrochemical enzymatic genosensor	Sequence of the SARS (severe acute respiratory syndrome) coronavirus (CoV) SARS-CoV/3 base mismatch 30-mer 3′-thiolated DNA strand	2.7530 ± 0.2030	na	na	na	na	Abad-Valle et al. (2007a,b)
Electrochemical detection	*p*-aminophenylbutyrate/ esterase 2 from *Alicyclobacillus acidocaldarius* plus oligodeoxynucleotide (ODN) in a site-specific manner (perfectly matched; ODN-P)	1.4252 ± 0.2030	0.4432 ± 0.2182	2.5556 ± 0.1208	na	0.5014 ± 0.1011	Wang et al. (2007)
Electrochemical detection	*p*-aminophenylbutyrate/ esterase 2 from *Alicyclobacillus acidocaldarius* plus oligodeoxynucleotide (ODN) in a site-specific manner (noncomplementary ODN; ODN-N)	0.5602 ± 0.2460	0. + 0.4148	1.78902 ± 0.2730	2.4304 ± 0.1647	na	Wang et al. (2007)

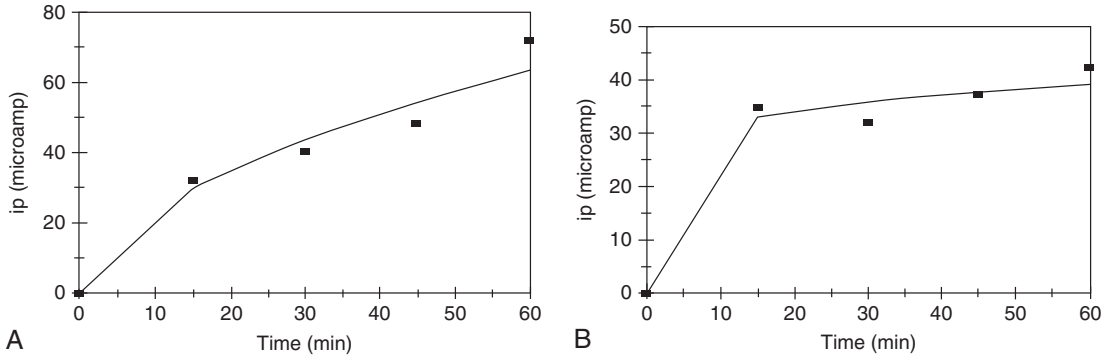

Figure 11.8

Binding (hybridization) of (a) complementary and (b) a noncomplementary (three-base mismatch strand) DNA in solution to a 30-mer 3′-thiolated DNA strand immobilized on an electrochemical enzymatic genosensor (Abad-Valle et al., 2007a,b)

Figure 11.8a shows the binding (hybridization) of a complementary DNA in solution to a 30-mer 3′-thiolated DNA strand immobilized on an electrochemical genosensor (Abad-Valle et al., 2007a,b). A single-fractal analysis is adequate to describe the binding kinetics. The values of the binding rate coefficient, k, and the fractal dimension, D_f, for a single-fractal analysis are given in Tables 11.4 and 11.5.

Figure 11.8b shows the binding (hybridization) of a three-base mismatch DNA strand to a 30-mer 3′-thiolated DNA strand immobilized on an electrochemical genosensor (Abad-Valle et al., 2007a,b). Once again a single-fractal analysis is adequate to describe the binding kinetics. The values of the binding rate coefficient, k, and the fractal dimension, D_f, for a single-fractal analysis are given in Tables 11.4 and 11.5. It is of interest to note that as one goes from the binding of the complementary DNA to the three base-mismatch strand in solution to the 30-mer 3′-thiolated DNA strand immobilized on the electrochemical genosensor, the fractal dimension increases by a factor of 1.427 from a value of D_f equals to 1.9290 to 2.7520, and the binding rate coefficient, k increases by a factor of 3.353 from a value of k equal to 7.0291 to k equal to 23.569. Increases in the degree of heterogeneity or the fractal dimension on the sensor chip surface and in the binding rate coefficient are in the same direction.

Wang et al. (2007) recently analyzed the binding of complementary ODN (ODN-P) (2-diolgonucleotide) and a noncomplementary ODN-N (nonmatching) to an electrochemical sensor with a EST2-A34 reporter. These authors used esterase 2-oligonucleotide conjugate as a sensitive reporter for the electrochemical detection of nucleic acid hybridization. Figure 11.9a shows the binding of *p*-aminophenylbutyrate/esterase 2 from *Alicyclobacillus acidocaldarius* plus oligonucleotide (ODN) in solution to a site-specific manner ODN-P (perfectly matched; complementary) immobilized on an electrochemical biosensor surface. A dual-fractal analysis is required to adequately describe the binding kinetics. A single-fractal

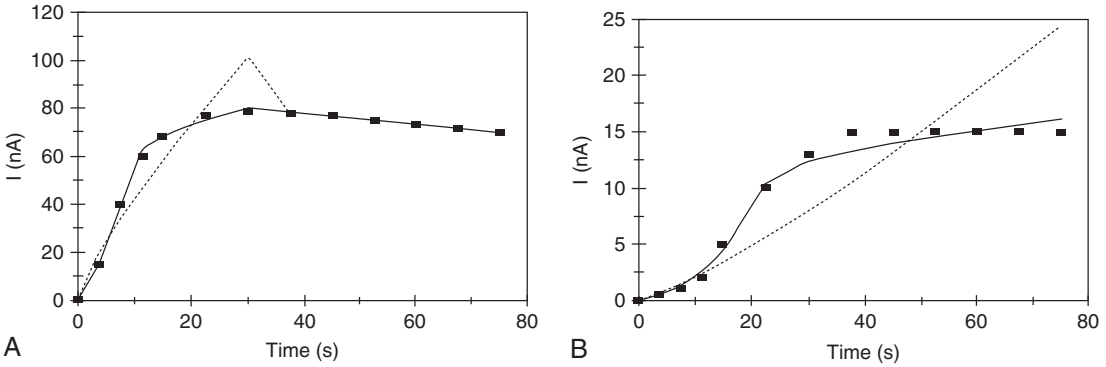

Figure 11.9

Binding (hybridization) of (a) a perfectly matched ODN (ODN-P) and (b) a noncomplementary ODN (ODN-N) to an electrochemical sensor with a EST2-A34 reporter (Wang et al., 2007). When a solid line is only used then a single-fractal analysis applies. When only a solid line (—) is used then a single-fractal analysis applies. When both a dashed (- - -) and a solid (—) line are used then the dashed line represents a single-fractal analysis and the solid line represents a dual-fractal analysis. In Figure (b) a single- and a triple-fractal analysis is shown.

analysis is required to adequately describe the dissociation kinetics. The values of (a) the binding rate coefficient, k, and the fractal dimension, D_f, for a single-fractal analysis, (b) the binding rate coefficients, k_1 and k_2, and the fractal dimensions, D_{f1} and D_{f2}, for a dual-fractal analysis, and (c) the dissociation rate coefficient, k_d, and the fractal dimension, D_{fd}, for a single-fractal analysis are given in Tables 11.4 and 11.5. It is of interest to note that for a dual-fractal analysis, as the fractal dimension increases by a factor of 5.766 from a value of D_{f1} equal 0.4432 to D_{f2} equal to 2.556, the binding rate coefficient increases by a factor of 13.25 from a value of k_1 equal to 2.8403 to k_2 equal to 37.626. Increases in the degree of heterogeneity or the fractal dimension on the electrochemical biosensor surface and in the binding rate coefficient are in the same direction.

Figure 11.9b shows the binding of *p*-aminophenylbutyrate/esterase 2 from *Alicyclobacillus acidocaldarius* plus ODN in solution to a site-specific manner ODN-N (mismatch; noncomplementary) immobilized on an electrochemical biosensor surface. In this case, a triple-fractal analysis is required to adequately describe the binding kinetics. The values of (a) the binding rate coefficient, k, and the fractal dimension, D_f, for a single-fractal analysis, (b) the binding rate coefficients, k_1 and k_2, and the fractal dimensions, D_{f1} and D_{f2}, for a dual-fractal analysis, and (c) the binding rate coefficients, k_1, k_2, and k_3, and the fractal dimensions, D_{f1}, D_{f2} and D_{f3}, for a triple-fractal analysis are given in Tables 11.4 and 11.5. The binding kinetics is a bit more complicated in this case (ODN-N; noncomplementary) when compared to the complementary (ODN-P) case, as for the ODN-N case a triple-fractal analysis is required to adequately describe the binding kinetics whereas for the complementary (ODN-P) case a dual-fractal analysis is adequate to describe the binding kinetics. It is of interest to note that for a triple-fractal analysis, as the fractal dimension increases by a factor of 1.358 from a value

of D_{f2} equal 1.78902 to D_{f3} equal to 2.4304, the binding rate coefficient increases by a factor of 3.03 from a value of k_2 equal to 1.5596 to k_3 equal to 4.7240. Increases in the degree of heterogeneity or the fractal dimension on the electrochemical biosensor surface and in the binding rate coefficient are once again in the same direction.

Uno et al. (2007) recently developed a peptide-nucleic acid (PNA)-modified IS-FET-based biosensor that they have used for the direct detection of DNA hybridization. These authors report that their IS-FET based biosensor uses the change in the surface potential on the hybridization of a negatively charged DNA. They explain that the use of PNA in their system permits the highly specific and selective binding at low ionic strength. Uno et al. (2007) point out that IS-FET based biological sensors are attractive in the sense that they are of small size and weight, provide a fast response, are portable, can be mass produced at a low cost, and are highly reliable. They further report that IS-FET-based DNA sensors have exhibited potential in clinical and research applications. Uno et al. (2007) report that the IS-FET can detect surface potential changes due to the surface adsorption of charged molecules in an aqueous environment (Souteyrand et al., 1997; Berney et al., 2000; Frits et al., 2002; Kim et al., 2004; Li et al., 2004). Uno et al. (2004) and Ohtake et al. (2004) have shown that the hybridization of an immobilized PNA with a complementary DNA induces a decrease in the saturation current and a positive shift in the threshold voltage.

Figure 11.10a shows the binding of 5 μM target DNA2 (complementary to CYP2C9*2) in solution to CYP2C9*2 used as a probe and immobilized on a SPR biosensor surface (Uno et al., 2007). This permitted these authors to analyze the molecular recognition at the solution-surface interface. A single-fractal analysis is adequate to describe the binding and the dissociation kinetics. The values of (a) the binding rate coefficient, k, and the fractal dimension, D_f, for a single-fractal analysis, and (b) the dissociation rate coefficient, k_d, and the fractal dimension, D_{fd}, for a single-fractal analysis are given in Table 11.6(a) and (b). In this case, the affinity, K ($=k/k_d$) value is 30,347.2 (an extremely high value).

Figure 11.10b shows the binding of 5 μM target DNA with a single base mismatch 2 (complementary to CYP2C9*2) in solution to CYP2C9*2 used as a probe and immobilized on a SPR biosensor surface (Uno et al., 2007). A single-fractal analysis is once again adequate to describe the binding and the dissociation kinetics. The values of (a) the binding rate coefficient, k, and the fractal dimension, D_f, for a single-fractal analysis, and (b) the dissociation rate coefficient, k_d, and the fractal dimension, D_{fd}, for a single-fractal analysis are given in Table 11.6(a) and (b). In this case, the affinity, K ($=k/k_d$), value is 229.54. It is of interest to note that as the fractal dimension decreases by 2.26% from a value of D_f equal to 2.6306 to 2.5712 the binding rate coefficient, k also decreases by 56.3% from a value of k equal to 131.10 to 57.253. Note that changes in the binding rate coefficient, k, and the fractal dimension, D_f, or the degree of heterogeneity on the sensor surface are in the same direction.

Figure 11.10c shows the binding of 5 μM target complementary DNA (complementary to CYP2C9*2) in solution to CYP2C9*2 used as a probe with a single mismatch (CYP2C9*1)

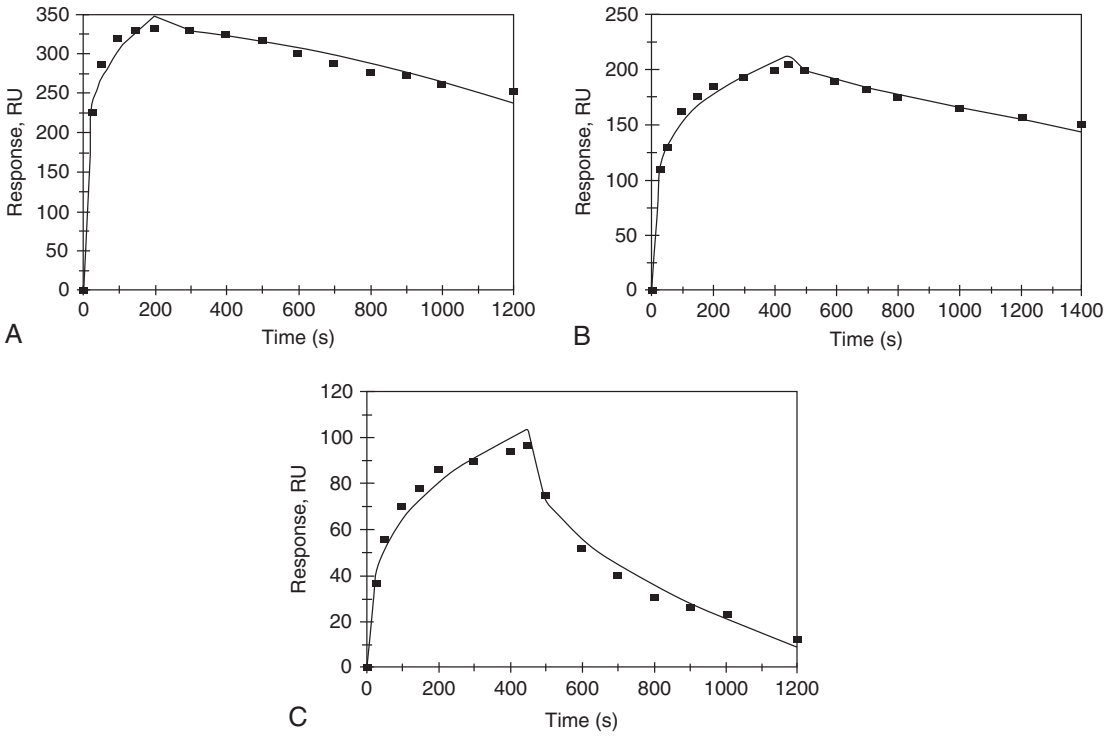

Figure 11.10

Binding and dissociation (hybridization) of 5 μM target in solution (a) complementary to CYP2C9*2, (b) with a single base mismatch to CYP2C9*2 immobilized on an ion-sensitive field-effect transistor-based biosensor, and (c) 5 μM target DNA in solution to a single-mismatch DNA, CYP2C9*1 immobilized on an ion-sensitive field-effect transistor-based biosensor (Uno et al., 2007).

and immobilized on a SPR biosensor surface (Uno et al., 2007). A single-fractal analysis is once again adequate to describe the binding and the dissociation kinetics. The values of (a) the binding rate coefficient, k, and the fractal dimension, D_f, for a single-fractal analysis, and (b) the dissociation rate coefficient, k_d, and the fractal dimension, D_{fd}, for a single-fractal analysis are given in Table 11.6(a) and (b). In this case, the affinity, K ($=k/k_d$), value is 3.954.

Figure 11.11a and Table 11.6(a) and (b) show the increase in the binding rate coefficient, k, with an increase in the fractal dimension, D_f, for a single-fractal analysis. For the data shown in Figure 11.11a and Table 11.6(a) and (b), the binding rate coefficient, k, is given by:

$$k = (4.6 \times 10^{-07} \pm 1.7 \times 10^{-07}) D_f^{10.91 \pm 3.59} \tag{11.5a}$$

The fit is reasonable. Only three data points are available. The availability of more data points would lead to a more reliable fit. The binding rate coefficient, k, for a single-fractal analysis is very sensitive to the fractal dimension, D_f, or the degree of heterogeneity that

Table 11.6: (a) Binding and dissociation rate coefficients and (b) fractal dimensions for the binding and the dissociation phases for PNA-DNA hybridization (a) 5 μM target DNA in solution complementary to CYP2C9*2 as a probe PNA immobilized on a nucleic acid-modified ion-selective field-effect transistor-based biosensor, and (b) target DNA in solution complementary to CYP2C9*2 and with involvement of a single mismatch in either the target DNA or the probe PNA immobilized on the nucleic acid-modified ion-selective field-effect transistor-based biosensor (Uno et al., 2007).

(a)		
Analyte in Solution/Receptor on Surface	k	k_d
5 μM target DNA complementary to receptor, CYP2C9*2/probe PNA, CYP2C9*2	131.10 ± 8.02	0.00432 ± 0.00099
Target DNA with single base mismatch/probe PNA, CYP2C9*2	57.253 ± 2.398	0.2496 ± 0.0310
Target DNA complementary to receptor/Probe PNSA, CYP2C9*2 with a single mismatch	15.429 ± 1.369	3.9020 ± 0.344
(b)		
Analyte in Solution/Receptor on Surface	D_f	D_{fd}
5 μM target DNA complementary to receptor, CYP2C9*2/probe PNA, CYP2C9*2	2.6306 ± 0.0730	0.00432 ± 0.00099
Target DNA with single base mismatch/probe PNA, CYP2C9*2	2.5712 ± 0.00304	0.2496 ± 0.0310
Target DNA complementary to receptor/Probe PNSA, CYP2C9*2 with a single mismatch	2.6306 ± 0.0703	0.102 + 0.179

exists on the biosensor surface as noted by the close to eleventh (equal to 10.91) order of dependence exhibited.

Figure 11.11b and Table 11.6(a) and (b) show the increase in the dissociation rate coefficient, k_d with an increase in the fractal dimension, D_{fd}, for a single-fractal analysis. For the data shown in Figure 11.11a and Table 11.6(a) and (b), the dissociation rate coefficient, k_d, is given by:

$$k_d = (0.3678 + 1.10262)D_{fd}^{2.007\pm0.6065} \tag{11.5b}$$

The fit is not good. Only three data points are available. The availability of more data points would lead to a more reliable fit. The dissociation rate coefficient, k_d, for a single-fractal analysis exhibits very close to a second (equal to 2.007) order of dependence on the fractal dimension, D_{fd}, or the degree of heterogeneity that exists in the dissociation phase on the biosensor surface.

Figure 11.11c and Table 11.6(a) and (b) show the increase in the affinity, K ($=k/k_d$), with an increase in the ratio of the fractal dimensions in the binding and in the dissociation phases (D_f/D_{fd}), for a single-fractal analysis. For the data shown in Figure 11.11a and Table 11.6(a) and (b), the affinity, K, is given by:

$$K(=k/k_d) = (13.6 + 124.34)(D_f/D_{fd})^{1.746\pm0.978} \tag{11.5c}$$

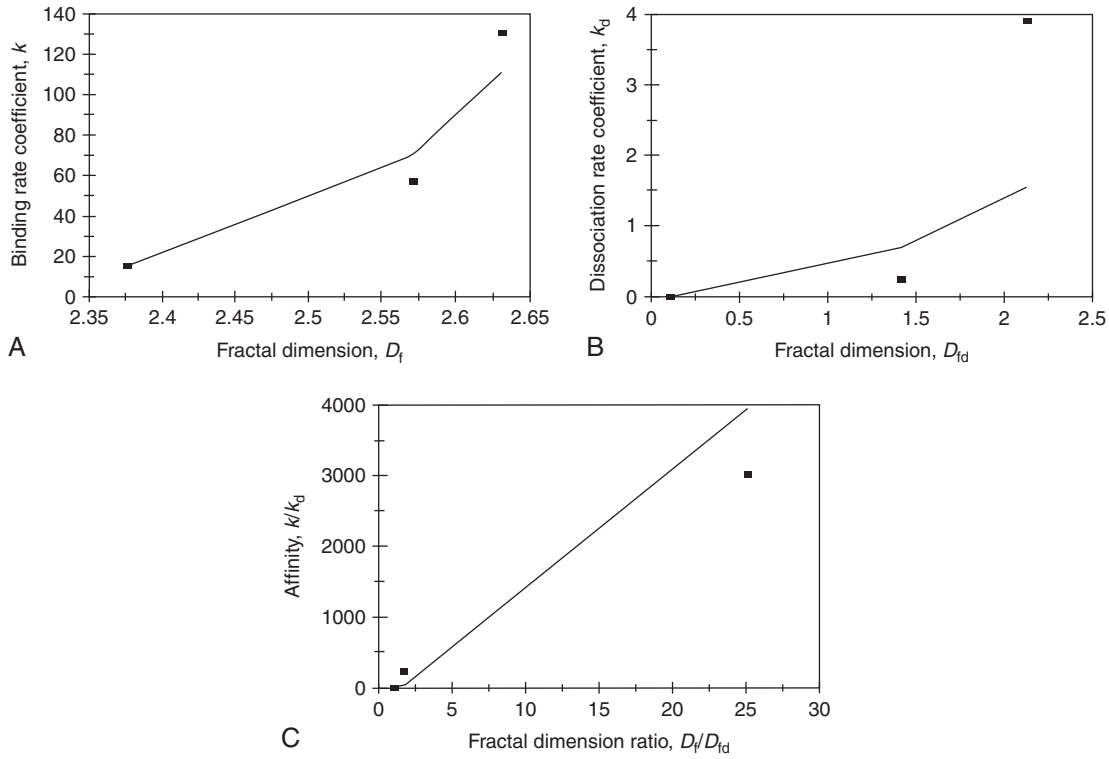

Figure 11.11

(a) Increase in the binding rate coefficient, k, with an increase in the fractal dimension, D_f. (b) Increase in the dissociation rate coefficient, k_d, with an increase in the fractal dimension in the dissociation phase, D_{fd}. (c) Increase in the affinity, K ($=k/k_d$), with an increase in the fractal dimension ratio, D_f/D_{fd}.

The fit is reasonable. Only three data points are available. The availability of more data points would lead to a more reliable fit. Only the positive error is shown in Equation (11.5c), since the error is large, and the affinity can only have positive values. The affinity, K, exhibits an order of dependence between one and a half and two (equal to 1.746) on the ratio of fractal dimensions, (D_f/D_{fd}), present on the sensor chip surface.

Uno et al. (2007) analyzed the SPR biosensor responses to PNA-DNA hybridization. These authors used CYP2C9*2 as the probe PNA and the target DNA was complementary CYP2C9*2 (target DNA2). They used target DNA concentrations in the 0.1-5.0 μM range. Figure 11.12a shows the binding and the dissociation of 5 μM target DNA concentration in solution to the probe PNA immobilized on the sensor surface. A dual-fractal analysis is required to adequately describe the binding kinetics. A single-fractal analysis is adequate to describe the dissociation kinetics. The values of (a) the binding rate coefficient, k, and the fractal dimension, D_f, for a single-fractal analysis, (b) the binding rate coefficients,

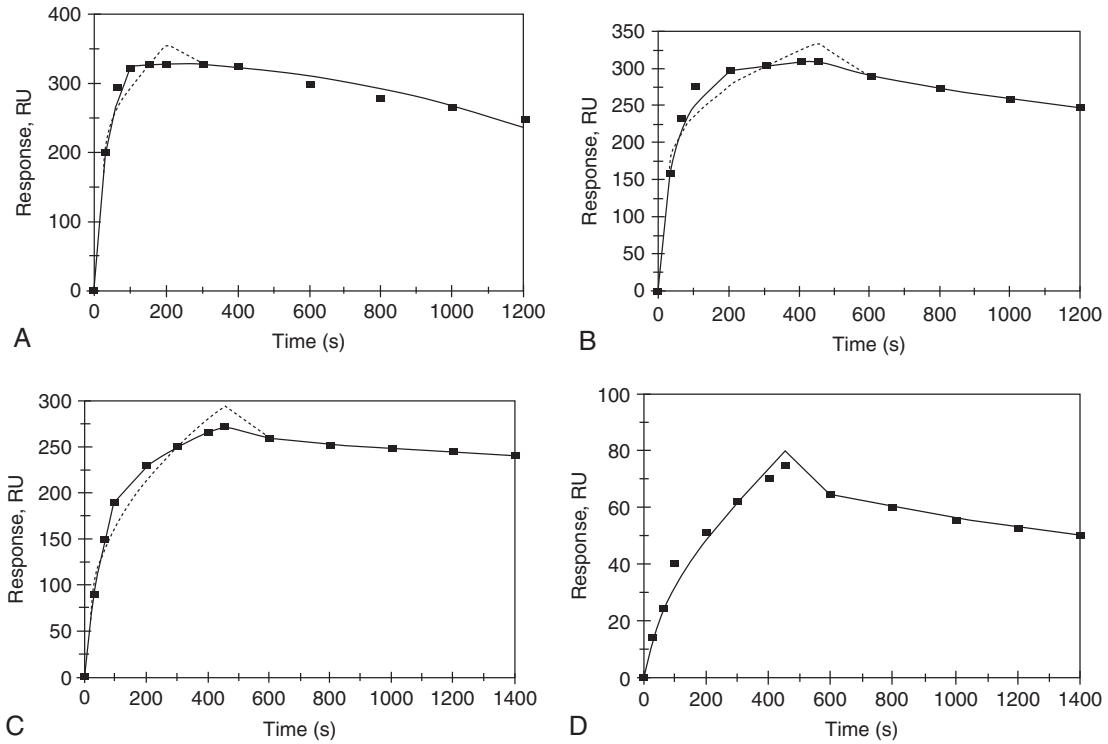

Figure 11.12

Binding and dissociation during PNA-DNA hybridization. Binding of different concentrations (in μM) of target DNA complementary to CYP2C9*2 (target DNA2) to CYP2C9*2 as a probe PNA immobilized on a ion-sensitive field-effect transistor-based biosensor (Uno et al.,2007): (a) 5. (b) 2.5. (c) 1. (d) 0.1. When only a solid line (—) is used then a single-fractal analysis applies. When both a dashed (- - -) and a solid (—) line are used then the dashed line represents a single-fractal analysis and the solid line represents a dual-fractal analysis.

k_1 and k_2, and the fractal dimensions, D_{f1} and D_{f2}, for a dual-fractal analysis, and (c) the dissociation rate coefficient, k_d, and the fractal dimension, D_{fd}, for the dissociation phase for a single-fractal analysis are given in Tables 11.7 and 11.8. Note that for a dual-fractal analysis, as the fractal dimension increases by 38.9% from a value of D_{f1} equal to 2.1140 to D_{f2} equal to 2.9360, the binding rate coefficient increases by a factor of 6.40 from a value of k_1 equal to 43.465 to k_2 equal to 278.35. Note that changes in the fractal dimension or the degree of heterogeneity on the sensor chip surface and in the binding rate coefficient are in the same direction.

Figure 11.12b shows the binding and the dissociation of 2.5 μM target DNA concentration in solution to the probe PNA immobilized on the sensor surface. Once again, a dual-fractal analysis is required to adequately describe the binding kinetics. A single-fractal analysis is adequate to describe the dissociation kinetics. The values of (a) the binding rate coefficient, k, and the fractal dimension, D_f, for a single-fractal analysis, (b) the binding rate coefficients,

Table 11.7: Binding and dissociation rate coefficients for different target complementary DNA concentrations (in μM) in solution to a DNA probe, CYP29*2 immobilized on an ion-sensitive field-effect transistor (IS-FET)-based biosensor (Uno et al., 2007).

Complementary DNA Concentration in Solution (μM)	k	k_1	k_2	k_d
5	85.694 ± 9.653	43.465 ± 3.303	278.35 ± 1.34	0.000256 ± 0.000118
2.5	82.808 ± 9.833	49.086 ± 5.681	225.0 ± 0.6886	0.6096 ± 0.0056
1.0	26.792 ± 3.322	8.427 ± 0.302	74.183 ± 0.174	1.864 ± 0.092
0.1	1.847 ± 0.255	na	na	0.8969 ± 0.126

Table 11.8: Fractal dimensions for the binding and the dissociation phases for the different target complementary DNA concentrations (in μM) in solution to a DNA probe, CYP29*2 immobilized on an ion-sensitive field-effect transistor (ISFET)-based biosensor (Uno et al., 2007).

Complementary DNA Concentration in Solution (μM)	D_f	D_{f1}	D_{f2}	D_{fd}
5	2.4606 ± 0.1505	2.1140 ± 0.1856	2.9360 ± 0.01941	0. + 0.3388
2.5	2.5416 ± 0.09368	2.2890 ± 0.1675	2.8933 ± 0.00977	1.6066 ± 0.0150
1.0	2.2146 ± 0.09662	1.2392 ± 0.08908	2.5728 ± 0.00748	2.1800 ± 0.06648
0.1	1.7662 ± 0.1066	na	na	2.0364 ± 0.01924

k_1 and k_2, and the fractal dimensions, D_{f1} and D_{f2}, for a dual-fractal analysis, and (c) the dissociation rate coefficient, k_d, and the fractal dimension, D_{fd}, for the dissociation phase for a single-fractal analysis are given in Tables 11.7 and 11.8. Note that for a dual-fractal analysis, as the fractal dimension increases by 26.4% from a value of D_{f1} equal to 2.2890 to D_{f2} equal to 2.8933, the binding rate coefficient increases by a factor of 4.58 from a value of k_1 equal to 49.086 to k_2 equal to 225.0. Note that changes in the fractal dimension or the degree of heterogeneity on the sensor chip surface and in the binding rate coefficient are once again in the same direction.

Figure 11.12c shows the binding and the dissociation of 1 μM target DNA concentration in solution to the probe PNA immobilized on the sensor surface. Once again, a dual-fractal analysis is required to adequately describe the binding kinetics. A single-fractal analysis is adequate to describe the dissociation kinetics. The values of (a) the binding rate coefficient, k, and the fractal dimension, D_f, for a single-fractal analysis, (b) the binding rate coefficients, k_1 and k_2, and the fractal dimensions, D_{f1} and D_{f2}, for a dual-fractal analysis, and (c) the dissociation rate coefficient, k_d, and the fractal dimension, D_{fd}, for the dissociation phase for a single-fractal analysis are given in Tables 11.7 and 11.8. Note that for a dual-fractal analysis, as the fractal dimension increases by a factor of 2.076 from a value of D_{f1} equal to 1.2392 to D_{f2} equal to 2.5728, the binding rate coefficient increases by a factor of 8.80 from a value of

k_1 equal to 8.427 to k_2 equal to 74.183. It is seen that changes in the fractal dimension or the degree of heterogeneity on the sensor chip surface and in the binding rate coefficient are once again in the same direction.

Figure 11.12d shows the binding and dissociation of 0.1 μM target DNA concentration in solution to the probe PNA immobilized on the sensor surface. A single-fractal analysis is adequate to describe the binding and the dissociation kinetics. The values of (a) the binding rate coefficient, k, and the fractal dimension, D_f, for a single-fractal analysis, and (b) the dissociation rate coefficient, k_d, and the fractal dimension, D_{fd}, for a single-fractal analysis are given in Tables 11.7 and 11.8. In this case, the affinity, K ($=k/k_d$), is given by 1.046. No reason is given at present as to why at this lowest DNA target concentration (0.1 μM) in solution a single-fractal analysis is adequate to describe the binding kinetics, whereas at the higher DNA concentration in solution in the 1.0-5.0 μM range, a dual-fractal analysis is required to adequately describe the binding kinetics.

In the entire 0.1-5.0 μM target concentration range a single-fractal analysis is adequate to describe the dissociation kinetics.

Figure 11.13a and Table 11.7 show the increase in the binding rate coefficient, k_1, with an increase in the target DNA concentration in the 1.0-5.0 μM range in solution for a dual-fractal analysis. For the data shown in Figure 11.13a, the binding rate coefficient, k_1, is given by:

$$k_1 = (10.67 \pm 10.27)[\text{target DNA}]^{1.067 \pm 0.590} \tag{11.6a}$$

The fit is not good. There is scatter in the data, and this is reflected in the error in the value of the binding rate coefficient, k_1. The binding rate coefficient, k_1, exhibits close to a first (equal to 1.067) order of dependence on the target DNA concentration in solution. The nonintegral order of dependence exhibited by the binding rate coefficient, k_1, lends support to the fractal nature of the system.

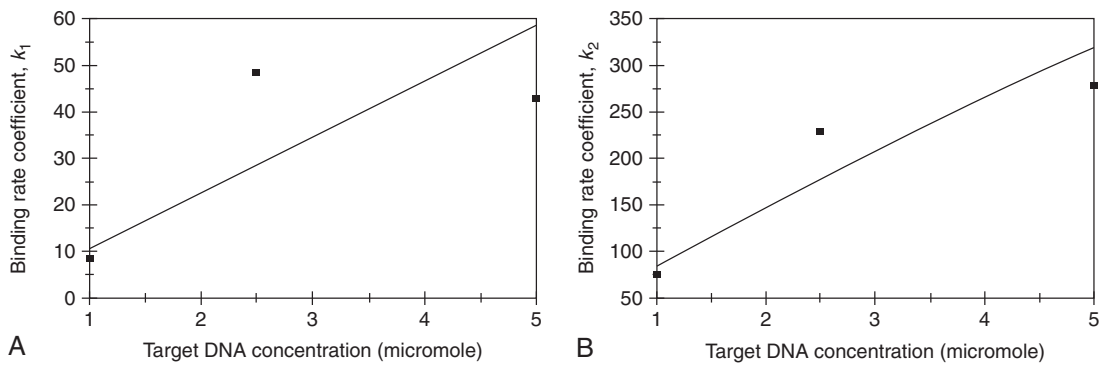

Figure 11.13
Increase in the binding rate coefficient (a) k_1 and (b) k_2 with an increase in the target DNA concentration in (in micromole) in solution.

Figure 11.13b and Table 11.7 show the increase in the binding rate coefficient, k_2, with an increase in the target DNA concentration in the 1.0-5.0 μM range in solution for a dual-fractal analysis. For the data shown in Figure 11.13b the binding rate coefficient, k_2, is given by:

$$k_2 = (82.13 \pm 27.67)[\text{target DNA}]^{0.842 \pm 0.254} \tag{11.6b}$$

The fit is reasonable. There is some scatter in the data. The binding rate coefficient, k_2, exhibits an order of dependence between a half and one (equal to 0.842) on the target DNA concentration in solution. The nonintegral order of dependence exhibited by the binding rate coefficient, k_1, once again lends support to the fractal nature of the system.

It is seen that the binding rate coefficient, k_2, exhibits an order of dependence less than one (equal to 0.842) on the target DNA concentration in solution., and the binding rate coefficient, k_1, exhibits an order of dependence greater than one (equal to 1.067) on the target DNA concentration in solution.

Figure 11.14a and Tables 11.7 and 11.8 show the increase in the binding rate coefficient, k_1, with an increase in the fractal dimension, D_{f1} for a dual-fractal analysis. For the data shown in Figure 11.4a, the binding rate coefficient, k_1, is given by:

$$k_1 = (4.517 \pm 0.377)D_{f1}^{2.944 \pm 0.1698} \tag{11.7a}$$

The fit is good. Only three data points are available. The availability of more data points would lead to a more reliable fit. The binding rate coefficient, k_1, is sensitive to the fractal dimension, D_{f1}, or the degree of heterogeneity that exists on the sensor chip surface as noted by the close to third (equal to 2.944) order of dependence exhibited.

Figure 11.14b and Tables 11.7 and 11.8 show the increase in the binding rate coefficient, k_2, with an increase in the fractal dimension, D_{f2}, for a dual-fractal analysis. For the data shown in Figure 11.4b, the binding rate coefficient, k_2, is given by:

$$k_2 = (0.00754 \pm 0.00038)D_{f2}^{9.734 \pm 0.48728} \tag{11.7b}$$

The fit is good. Only three data points are available. The availability of more data points would lead to a more reliable fit. The binding rate coefficient, k_2, is extremely sensitive to the fractal dimension, D_{f2}, or the degree of heterogeneity that exists on the sensor chip surface as noted by the order of dependence between nine and a half and ten (equal to 9.734) exhibited. No explanation is offered at present to help explain this extremely very high order of dependence exhibited.

Figure 11.14c and Tables 11.7 and 11.8 show the increase in the ratio of the binding rate coefficients, k_2/k_1, with an increase in the fractal dimension ratio, D_{f2}/D_{f1}, for a dual-fractal

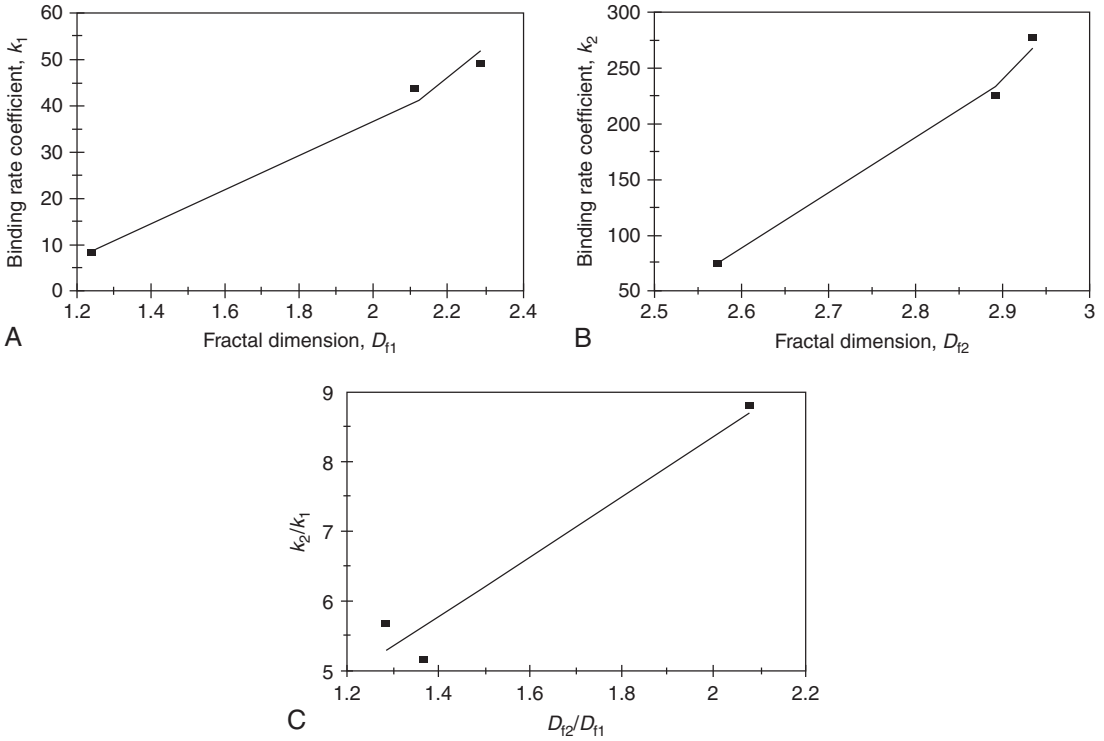

Figure 11.14

(a) Increase in the binding rate coefficient, k_1, with an increase in the fractal dimension, D_{f1}
(b) Increase in the binding rate coefficient, k_2, with an increase in the fractal dimension, D_{f2}
(c) Increase in the ratio of the binding rate coefficients, k_2/k_1, with an increase in the ratio of the fractal dimensions, D_{f2}/D_{f1}.

analysis. For the data shown in Figure 11.14c the ratio of the binding rate coefficients, k_2/k_1, is given by:

$$k_2/k_1 = (4.063 \pm 0.486)(D_{f2}/D_{f1})^{1.043\pm0.306} \tag{11.7c}$$

The fit is good. Only three data points are available. The availability of more data points would lead to a more reliable fit. The ratio of binding rate coefficients, k_2/k_1, exhibits close to a first (equal to 1.043) order of dependence on the ratio of fractal dimensions, D_{f2}/D_{f1}, that exists on the sensor chip surface.

Figure 11.15a and Tables 11.7 and 11.8 show the increase in the fractal dimension, D_{f1}, with an increase in the target DNA concentration in solution in the 1-5 μM range. For the data shown in Figure 11.15a the fractal dimension, D_{f1}, is given by:

$$D_{f1} = (1.354 \pm 0.387)[\text{target DNA, in } \mu\text{M}]^{0.349\pm0.221} \tag{11.7d}$$

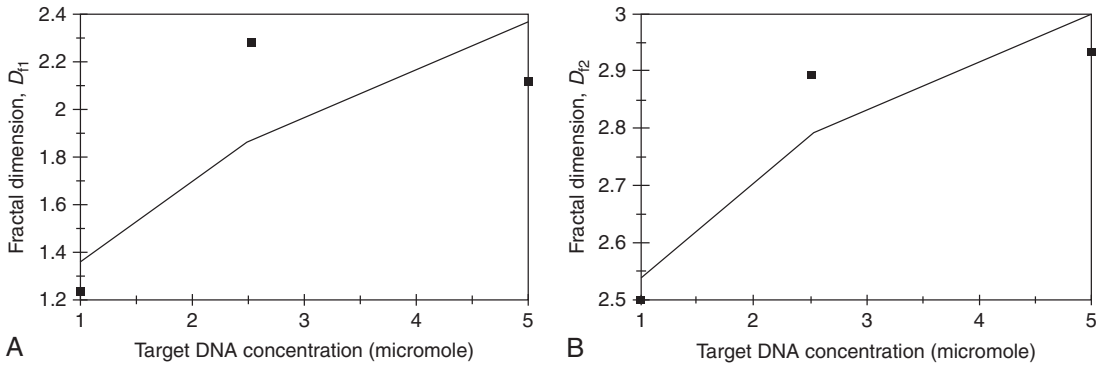

Figure 11.15

Increase in (a) the fractal dimension, D_{f1} and (b) the fractal dimension, D_{f2} with an increase in the target DNA concentration (in μM) in solution.

The fit is reasonable. There is scatter in the data. Only three data points are available. The availability of more data points would lead to a more reliable fit. The fractal dimension, D_{f1}, exhibits only a very mild (equal to 0.349) order of dependence on the target DNA concentration in solution in the 1-5 μM range.

Figure 11.15b and Tables 11.7 and 11.8 show the increase in the fractal dimension, D_{f2}, with an increase in the target DNA concentration in solution in the 1-5 μM range. For the data shown in Figure 11.15b the fractal dimension, D_{f2}, is given by:

$$D_{f1} = (2.539 \pm 0.115)[\text{target DNA, in } \mu\text{M}]^{0.103 \pm 0064} \tag{11.7e}$$

The fit is reasonable. There is scatter in the data. Only three data points are available. The availability of more data points would lead to a more reliable fit. The fractal dimension, D_{f2}, exhibits only a very low (equal to 0.103) order of dependence on the target DNA concentration in solution in the 1-5 μM range. Note that the fractal dimension is based on a log scale, and even small changes in the fractal dimension lead to significant changes in the degree of heterogeneity on the sensor chip surface.

Blair et al. (2007) report that techniques have been used for the *in situ* quantification of DNA during enzymatic synthesis, for example, during a real-time polymerase chain reaction (Watzinger et al., 2006). Blair et al. (2007) point out that hybridization probes involving "molecular beacons" is a DNA quantification method. They have a stem-loop structure with complementary ends that anneal to each other. A fluorophore and a quencher are at opposite ends. Blair et al. (2007) explain that the loop structure is complementary to the target. Thus, as the beacon binds to the target, the fluorophore is separated from the quencher. This leads to an increase in the fluorescence, and is proportional to the amount of the DNA produced

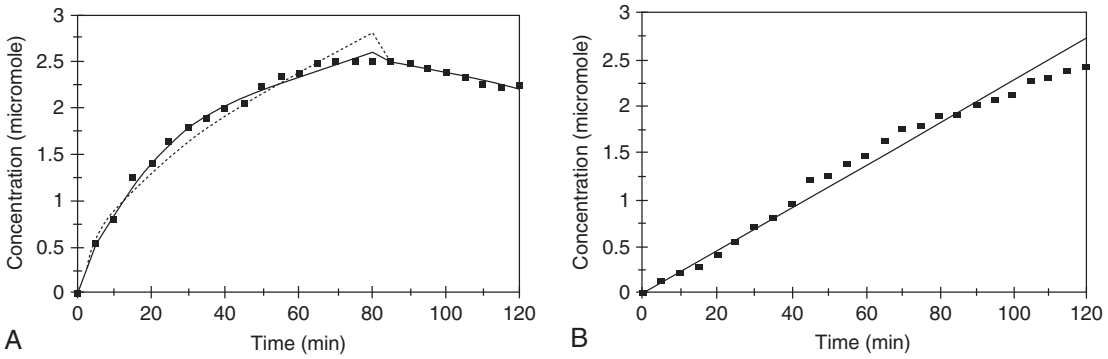

Figure 11.16

Binding and dissociation of RNA synthesized on a (a) 420 nM template and a (b) 42 nM template (Blair et al., 2007). When only a solid line (—) is used then a single-fractal analysis applies. When both a dashed (- - -) and a solid (—) line are used then the dashed line represents a single-fractal analysis and the solid line represents a dual-fractal analysis.

(Tyagi and Kramer, 1996; Leone et al., 1998; Guilietti et al., 2001; Summerer and Marx, 2002; Marras et al., 2006).

Blair et al. (2007) have developed a novel hybridization-based assay for the real-time monitoring of RNA synthesis. In their method complementary nucleotides were used to quantify the amount of RNA production by T7 polymerase. Figure 11.16a shows the binding and dissociation of RNA synthesized on a 420 nM template. The RNA concentration was determined by conversion using a calibration curve. A dual-fractal analysis is required to adequately describe the binding kinetics. A single-fractal analysis is adequate to describe the dissociation kinetics. The values of (a) the binding rate coefficient, k, and the fractal dimension, D_f, for a single-fractal analysis, (b) the binding rate coefficients, k_1 and k_2, and the fractal dimensions, D_{f1} and D_{f2}, for a dual-fractal analysis, and (c) the dissociation rate coefficient, k_d, and the fractal dimension for the dissociation phase, D_{fd}, for a single-fractal analysis are given in Tables 11.9 and 11.10. It is of interest to note that for a dual-fractal analysis as the fractal dimension increases by a factor of 1.35 from a value of D_{f1} equal to 1.6862 to D_{f2}r equal to 2.2812, the binding rate coefficient increases by a factor of 2.79 from a value of k_1 equal to 0.1909 to k_2 equal to 0.5324. The changes in the degree of heterogeneity on the sensor chip surface and in the binding rate coefficient are in the same direction.

Table 11.9: Binding and dissociation rate coefficients for (a) RNA synthesized on a 42 nM and a 420 nM template (Blair et al., 2007).

Template Concentration (nM)	k	k_1	k_2	k_d
420	0.2546 ± 0.0121	0.1909 ± 0.0121	0.5324 ± 0.0120	0.00204 ± 0.00031
42	0.02317 ± 0.00234	na	na	na

Table 11.10: Fractal dimensions in the binding and in the dissociation phase for (a) RNA synthesized on a 42 nM and a 420 nM template (Blair et al., 2007).

Template Concentration (nM)	D_f	D_{f1}	D_{f2}	D_{fd}
420	1.9086 ± 0.04988	1.6862 ± 0.07340	2.2812 ± 0.06678	0.2438 ± 0.1439
42	1.0136 ± 0.04822	na	na	na

Figure 11.16b shows the binding and dissociation of RNA synthesized on a 42 nM template. A single-fractal analysis is adequate to describe the binding kinetics. The values of the binding rate coefficient, k, and the fractal dimension, D_f, for a single-fractal analysis are given in Tables 11.9 and 11.10. Note that for the lower 42 nM template concentration a single-fractal analysis is adequate to describe the binding kinetics, whereas for the higher 420 nM template concentration a dual-fractal analysis is required to adequately describe the binding kinetics. This would seem to indicate that there is a change in the binding mechanism as one goes from the lower (42 nM template) to the higher (420 nM template) concentration.

Blair et al. (2007) analyzed the kinetics of displacement as a function of target concentration. These authors incubated the pre-hybridized 22-nt FQ (fluorophore quencher) complex with varying concentrations of the ss DNA target at 37 °C for 90 min. Figure 11.17a shows the binding of the 500 nM target ss DNAS (T) in solution in a "broken beacon" assay.

It is of interest to note that as the fractal dimension increases by a factor of 1.352 from a value of D_{f1} equal to 1.6862 to D_{f2} equal to 2.2812, the binding rate coefficient increases by a factor of 2.79 from a value of k_1 equal to 0.1909 to k_2 equal to 0.5324. The changes in the binding rate coefficient and in the fractal dimension or the degree of heterogeneity on the sensor chip surface are in the same direction.

Figure 11.17b shows the binding of the 250 nM target ss DNA (T) in solution in a "broken beacon" assay (Blair et al., 2007). A dual-fractal analysis is required to adequately describe the binding kinetics. The values of (a) the binding rate coefficient, k, and the fractal dimension, D_f, for a single-fractal analysis, and (b) the binding rate coefficients, k_1 and k_2, and the fractal dimensions, D_{f1} and D_{f2}, for a dual-fractal analysis are given in Tables 11.11 and 11.12.

Once again, it is of interest to note that as the fractal dimension increases by a factor of 1.129 from a value of D_{f1} equal to 2.5368 to D_{f2} equal to 2.9659, the binding rate coefficient increases by a factor of 1.60 from a value of k_1 equal to 17311.23 to k_2 equal to 27699.83. Once again, it is seen that changes in the binding rate coefficient and in the fractal dimension or the degree of heterogeneity on the sensor chip surface are in the same direction.

Tables 11.11 and 11.12 Binding rate coefficients and fractal dimensions for different concentrations of ss DNA concentration in solution pre-incubated with prehybridized 22-nt FQ duplex to the "broken beacon" (Blair et al., 2007)

ss DNA concentration in solution (in nM)	k	k_1	k_2	D_f	D_{f1}	D_{f2}
500 nM T	27162.52 ± 2112.81	24434.52 ± 2335.01	34530.40 ± 338.91	2.6996 ± 0.03036	2.5368 ± 0.08588	2.8285 ± 0.01352
250 nM T	18844.78 ± 1281.48	17311.23 ± 223.15	27699.83 ± 130.21	2.7582 ± 0.02608	2.6264 ± 0.01132	2.9659 ± 0.00629
100 nM T	10108.8 ± 949.88	9171.31 ± 492.50	14970.66 ± 21.90	2.7772 ± 0.03812	2.6278 ± 0.03964	2.9916 ± 0.00315

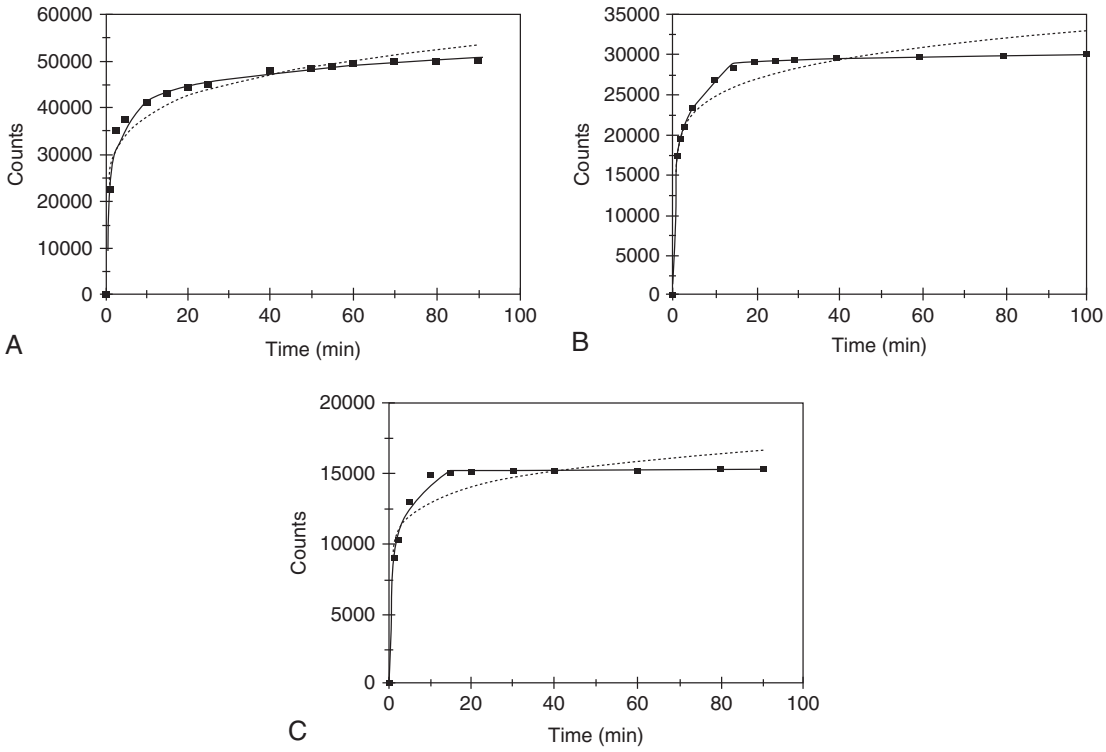

Figure 11.17

Binding (hybridization) of different concentrations of ss DNA in solution preincubated with prehybridized 22-nt FQ duplex to a "broken beacon" immobilized on a sensor surface (Blair et al., 2007): (a) 500 nM T. (b) 250 nM T. (c) 100 nM T. When only a solid line (—) is used then a single-fractal analysis applies. When both a dashed (- - -) and a solid (—) line are used then the dashed line represents a single-fractal analysis and the solid line represents a dual-fractal analysis.

Figure 11.17c shows the binding of the 100 nM target ss DNA (T) in solution in a "broken beacon" assay (Blair et al., 2007). A dual-fractal analysis is required to adequately describe the binding kinetics. The values of (a) the binding rate coefficient, k, and the fractal dimension, D_f, for a single-fractal analysis, and (b) the binding rate coefficients, k_1 and k_2, and the fractal dimensions, D_{f1} and D_{f2}, for a dual-fractal analysis are given in Tables 11.11 and 11.12.

Once again, it is of interest to note that as the fractal dimension increases by a factor of 1.138 from a value of D_{f1} equal to 2.6278 to D_{f2} equal to 2.9916, the binding rate coefficient increases by a factor of 1.632 from a value of k_1 equal to 9171.31 to k_2 equal to 14970.66. Once again, and as above, it is seen that changes in the binding rate coefficient and in the fractal dimension or the degree of heterogeneity on the sensor chip surface are in the same direction.

Figure 11.18a and Tables 11.11 and 11.12 show the increase in the binding rate coefficient, k_1, with an increase in the ss DNA concentration in solution in the 100-500 nM range. For the data shown in Figure 11.18a the binding rate coefficient, k_1, is given by:

$$k_1 = (556.51 \pm 36.18)[\text{ss DNA, in nM}]^{0.6132 \pm 0.05517} \tag{11.8a}$$

The fit is good. Only three data points are available. The availability of more data points would lead to a more reliable fit. The binding rate coefficient, k_1, exhibits an order of dependence between a half and one (equal to 0.6132) on the ss DNA concentration in solution in the 100-500 nM range. The nonintegral order of dependence exhibited lends support to the fractal nature of the system.

Figure 11.18b and Tables 11.11 and 11.12 show the increase in the binding rate coefficient, k_2, with an increase in the ss DNA concentration in solution in the 100-500 nM range. For the data shown in Figure 11.18b the binding rate coefficient, k_2, is given by:

$$k_2 = (1383.75 \pm 8.41)[\text{ss DNA, in nM}]^{0.5443 \pm 0.3197} \tag{11.8b}$$

The fit is good. Only three data points are available. The availability of more data points would lead to a more reliable fit. The binding rate coefficient, k_2, exhibits an order of dependence slightly more than a half (equal to 0.5443) order on the ss DNA concentration in solution in the 100-500 nM range. Once again, the nonintegral order of dependence exhibited lends support to the fractal nature of the system.

Figure 11.18c and Tables 11.11 and 11.12 show the decrease in the binding rate coefficient, k_1, with an increase in the fractal dimension, D_{f1}. For the data shown in Figure 11.18c the binding rate coefficient, k_1, is given by:

$$k_1 = (1.3 \times 10^{-12} \pm 0.8 \times 10^{-12}) D_{f1}^{-19.14 \pm 15.48} \tag{11.8c}$$

The fit is reasonable. Only three data points are available. The availability of more data points would lead to a more reliable fit. The binding rate coefficient, k_1, is extremely sensitive to the fractal dimension, D_{f1}, or the degree of heterogeneity that exists on the sensor surface as noted by the greater than nineteenth (equal to -19.14) order of dependence exhibited.

Figure 11.18d and Tables 11.11 and 11.12 show the decrease in the binding rate coefficient, k_2, with an increase in the fractal dimension, D_{f2}. For the data shown in Figure 11.18d the binding rate coefficient, k_2, is given by:

$$k_2 = (5.4 \times 10^{-12} \pm 2.3 \times 10^{-12}) D_{f2}^{-11.45 \pm 8.644} \tag{11.8d}$$

The fit is reasonable. Only three data points are available. The availability of more data points would lead to a more reliable fit. The binding rate coefficient, k_2, is extremely sensitive to the fractal dimension, D_{f2}, or the degree of heterogeneity that exists on the sensor

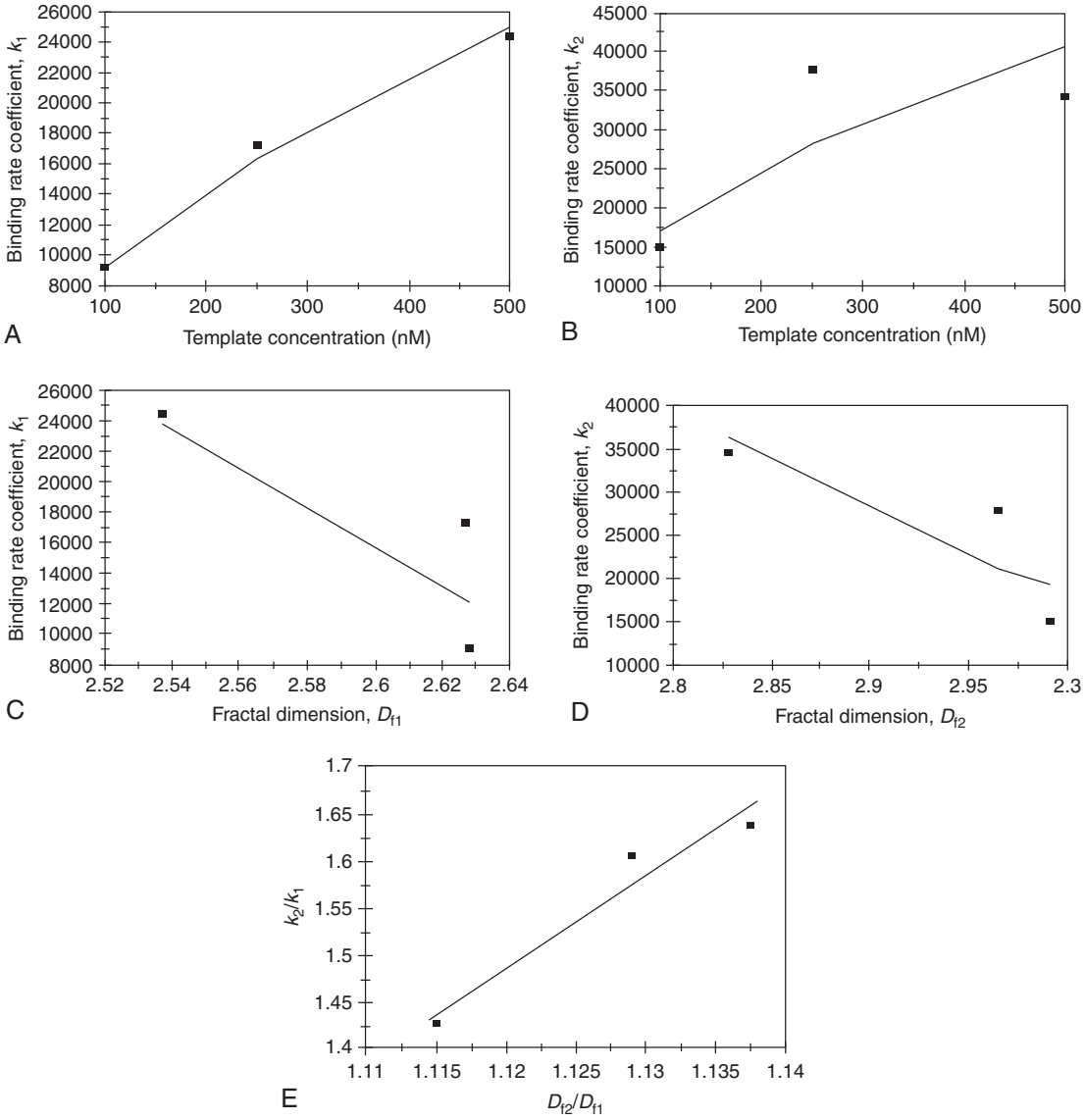

Figure 11.18

(a) Increase in the binding rate coefficient (a) k_1 and (b) k_2 with an increase in the template concentration (in nM) (c) Decrease in the binding rate coefficient, k_1, with an increase in the fractal dimension, D_{f1} (d) Decrease in the binding rate coefficient, k_2, with an increase in the fractal dimension, D_{f2} (e) Increase in the ratio of the binding rate coefficients, k_2/k_1, an increase in the ratio of the fractal dimensions, D_{f2}/D_{f1}.

surface as noted by the slightly less than negative eleven and a half (equal to −11.45) order of dependence exhibited.

Figure 11.18e and Tables 11.11 and 11.12 show the increase in the ratio of the binding rate coefficients, k_2/k_1, with an increase in the ratio of the fractal dimensions, D_{f2}/D_{f1}. For the data shown in Figure 11.18e the ratio of the binding rate coefficients, k_2/k_1, is given by:

$$k_2/k_1 = (0.653 \pm 0.019)D_{f2}/D_{f1}{}^{7.17\pm1.93} \tag{11.8e}$$

The fit is good. Only three data points are available. The availability of more data points would lead to a more reliable fit. The ratio of the binding rate coefficients, k_2/k_1, is very sensitive to the ratio of fractal dimensions, D_{f2}/D_{f1}, as noted by the order of dependence between seven and seven and a half (equal to 7.17) exhibited.

11.4 Conclusions

A fractal analysis is presented for the binding and dissociation of different analytes on arrays/microarrays/DNA chips. The analysis of both the binding as well as the dissociation (wherever applicable) provides a more complete picture of the reaction occurring on the sensor chip surface, besides providing for values of the affinities wherever applicable. This is the ratio of the rate coefficients in the binding and in the dissociation steps. The fractal analysis provides values of the binding rate coefficient, k, and the degree of heterogeneity made quantitative by the fractal dimension, D_f, on the sensor chip surface. The fractal analysis is applied to (a) the binding and dissociation (hybridization) of different targets (400 nM) in solution to a probe immobilized on a DNA chip surface (Fiche et al., 2007), (b) binding (hybridization) of different concentrations (in nM) of free-DNA in solution to a 22-mer strand (bound DNA) immobilized via a phenylene-diisocyanate linker molecule on a glass substrate (Michel et al., 2007), (c) binding (hybridization) of SA-HRP in solution to a capture probe on a QCM electrode along with a detecttion probe (Feng et al., 2007), (d) binding (hybridization) of a complementary and a noncomplementary (three-base mismatch strand) DNA in solution to a 30-mer 3′-thiolated DNA strand immobilized on an electrochemical enzymatic genosensor (Abad-Valle et al., 2007a,b), (e) binding (hybridization) of (i) a ODN-P and (ii) a noncomplementary ODN (ODN-N) to an electrochemical sensor with a EST2-A34 reporter (Wang et al., 2007), (f) binding and dissociation during PNA-DNA hybridization—binding of different concentrations (in μM) of target DNA complementary to CYP2C9*2 (target DNA2) to CYP2C9*2 as a probe PNA immobilized on a IS-FET-based biosensor (Uno et al., 2007), (g) binding and dissociation during PNA-DNA hybridization—binding of different concentrations (in μM) of target DNA complementary to CYP2C9*2 (target DNA2) to CYP2C9*2 as a probe PNA immobilized on an IS-FET-based biosensor (Uno et al., 2007), (h) binding and dissociation of RNA synthesized on a (i) 42 nM template and a (ii) 420 nM template (Blair et al., 2007), and (i) binding (hybridization) of different concentrations of ss DNA in solution pre-incubated with pre-hybridized 22-nt FQ duplex to a "broken beacon" immobilized on a sensor surface (Blair et al., 2007).

Both single- and dual-fractal analysis are used to adequately model the binding and dissociation kinetics. The dual-fractal analysis was used only when the single-fractal analysis did not provide an adequate fit (sum of least squares less than 0.97). This was done by the regression analysis provided by Corel Quattro Pro 8.0 (1997). The fractal analysis permits a link between the binding rate coefficient, k, and the degree of heterogeneity, D_f that exists on the biosensor surface. This provides a more complete picture of the reaction kinetics occurring on the sensor chip surface.

It is suggested that the fractal surface (roughness) leads to turbulence, which enhances mixing, decreases diffusional limitations, and leads to an increase in the binding rate coefficient (Martin et al., 1991). For this to occur, the characteristic length of the turbulent boundary layer may have to extend a few monolayers above the sensor chip surface to affect bulk diffusion to and from the surface. However, given the extremely laminar flow regimes in most biosensors this may not actually take place. The sensor chip (arrays/microarrays/DNA chips) surface is characterized by grooves and ridges, and this surface morphology may lead to eddy diffusion. This eddy diffusion can then help to enhance the mixing and extend the characteristic length of the boundary layer to affect the bulk diffusion to and from the surface.

The analysis of the different examples of the detection of analytes on arrays/microarrays/DNA chips should encourage experimentalists to pay more attention to the nature of the surface, and how it may be manipulated in desired directions. Detection of analytes on arrays/microarrays/DNA chips is bound to increase in the future as these "tools" find increasing applications in a wide variety of areas. This is of particular value primarily in the biomedical area, and also in other areas of application. For example, the identification of DNA sequences is of particular value in clinical pathology. A clinical pathologist is a medical doctor responsible for the diagnosis of diseases based on the analysis of body fluids, for example, blood and urine. The earlier one may detect and diagnose the probable onset of diseases the earlier one can begin the medical protocols necessary to help prevent, alleviate, or correct the onset of, especially, debilitating and intractable diseases. It is hoped that fractal analysis should be particularly helpful in providing a better understanding of the onset of diseases, particularly those that are insidious and debilitating. Any insight that is made available by such an analysis that helps in the management of intractable diseases should prove invaluable.

References

Abad-Valle P, MT Fernandez-Abedul, and A Costa-Garcia, DNA single-base mismatch study with an electrochemical enzymatic genosensor, *Biosensors & Bioelectronics*, **20**, 2251–2260 (2007a).

Abad-Valle P, MT Fernandez-Abedul, and A Costa-Garcia, DNA single-base mismatch study with an electrochemical enzymatic genosensor, *Biosensors & Bioelectronics*, **22**, 1642–1650 (2007b).

Blair RH, ES Rosenblum, ED Dawson, RD Kuchta, LR Kuck, and KL Rowlen, Real-time quantification of RNA polymerase activity using a "broken beacon", *Biosensors & Bioelectronics*, **22**, 213–220 (2007).

Caruana DJ and A Heller, Enzyme-amplified amperometric detection of hybridization and of a single-base pair mutation in an 18-base oligonucleotide on a 7 μm-diameter Electrode, *Journal of the American Chemical Society*, **121**, 769–774 (1999).

Feng K, J Li, JH Jiang, GL Shen, and RQ Yu, QCM detection with single-base mutation based on ligase reaction and biocatalyzed deposition amplification, *Biosensors & Bioelectronics*, **22**, 1651–1657 (2007).

Fiche JB, A Buhot, R Calemczuk, and T Livache, Temperature effects on DNA chip experiments from surface plasmon resonance imaging: Isotherms and melting curves, *Biophysical Journal*, **92**, 935–946 (2007).

Guilietti A, L Overbergh, D Valckx, B Decallonne, R Bouillon, and C Mathieu, An overview of real-time quantitative PCR: Applications to quantify cytokine gene expression, *Methods*, **25**, 386–401 (2001).

Havlin S, Molecular diffusion and reactions in *The Fractal Approach to Heterogeneous Chemistry: Surfaces, Colloids, Polymers* (ed. D Avnir), Wiley, New York, 1989, pp. 251–269.

Hekstra D, AR Taussig, M Magnasco, and F Naef, Absolute mRNA concentrations from sequence-specific calibration of oligonucleotide arrays, *Nucleic Acids*, **31**, 1962–1968 (2003).

Karousis NG, S Aouabdi, AS Way, and SM Reddy, Quartz crystal microbalance determination of organophosphorous and carbamate pesticides, *Analytica Chimica Acta*, **469**, 189–196 (2002).

Kim DS, YT Jeong, HK Cyu, HJ Park, HS Kim, JK Shin, P Choi, JH Lee, G Lim, and M Ishida, *Japan Journal of Applied Physics*, **42**, 4111–4115 (2003).

Landegren U, R Kaiser, J Sanders, and L Hood, A ligase-mediated gene detection technique, *Science*, **1241**, 1077–1080 (1988).

Lee CK and SL Lee, Multi-fractal scaling analysis of reactions over fractal surfaces, *Surface Science*, **325**, 294–310 (1995).

Leone G, H van Schijndel, B van Gemen, FR Kramer, and CD Schoen, Molecular beacon probes combined with amplification by NASBA enable homogeneous, real-time detection of RNA, *Nucleic Acid Research*, **26**, 2150–2155 (1998).

Ohtake T, C Hamai, T Uno, H Tabata, and T Kawai, *Japan Journal of Applied Physics*, **43**(9A/B), 11137–11139 (2004).

Marras SAE, S Tyagi, and FR Kramer, Real-time assays with molecular beacons and other fluorescence nucleic acid hybridization probes, *Clinica Chimica Acta*, **363**, 48–60 (2006).

Martin ST, VE Granstuff, and GC Frye, Effect of surface roughness on the response of thickness-shear mode resonators in liquids, *Analytical Chemistry*, **65**, 2910–2922 (1991).

Michel W, T Mai, T Naiser, and A Ott, Optical study of DNA surface hybridization reveals DNA surface density as a key parameter for microarray hybridization kinetics, *Biophysical Journal*, **92**, 994–1004 (2007).

Peterson AW, LK Wolf, and RM Georgiadis, Hybridization of mismatched or partially matched DNA at surfaces, *Journal of the American Chemical Society*, **124**, 14601–14607 (2002).

Summerer D and A Marx, A molecular beacon for quantitative monitoring of the DNA polymerase reaction in real-time, *Angew Chemistry International Edition*, **41**, 3620–3622 (2002).

Tawa K and W Knoll, Mismatching base-pair dependence of the kinetics of DNA-DNA hybridization studied by surface plasmon resonance fluorescence spectroscopy, *Nucleic Acids Research*, **32**, 2372–2377 (2004).

Tyagi S and FR Kramer, Molecular beacons: Probes that fluoresce upon hybridization, *Nature Biotechnology*, **14**, 303–308 (1996).

Uno T, T Ohtake, H Tabata, and T Kawai, *Japan Journal of Applied Physics*, **43**(12B), 11584–11587 (2004).

Uno T, H Tabata, and T Kawai, Peptide-nucleic acid-modified ion-sensitive field-effect based biosensor for direct detection of DNA hybridization, *Analytical Chemistry*, **79**, 52–59 (2007).

Wabuyele MB, H Farquar, W Stryjewski, RP Hammer, SA Sofer, YW Cheng, and F Barany, Approaching real-time molecular diagnostics: Single-pair fluorescence energy transfer (spFRET) detection for the analysis of low abundant point mutations in K-ras oncogenes, *Journal of the American Chemical Society*, **125**, 6937–6945 (2003).

Wang Y, W Gumbrecht, M Humenik, and M Sprinzl, Esterase 2-oligonucleotide conjugates as sensitive reporter for electrochemical detection of nucleic acid hybridization, *Biosensors & Bioelectronics*, **22**, 1798–1806 (2007).

Wark AW, HJ Lee, and RM Corn, Long-range surface plasmon resonance imaging for bioaffinity sensors, *Analytical Chemistry*, **77**, 3904–3907 (2005).

Watzinger F, K Ebner, and T Lion, Detection and monitoring of virus infections by real-time PCR, *Molecular Aspects of Medicine*, **27**, 254–298 (2006).

Yao D, J Kim, F Yu, PE Nielson, EK Sinner, and W Knoll, Surface density dependence of PCR amplicon hybridization on PN1/DNA probe layers, *Biophysical Journal*, **88**, 2745–2751 (2005).

Yu F, D Yao, and W Knoll, Oligonucleotide hybridization studied by a surface plasmon resonance diffraction sensor (SPDS), *Nucleic Acids Research*, **32**, e75 (2004).